Supporting Information

Dual Supramolecular Chirogenesis Based on Platinum(II) Metallotweezers

Jie Ren,[a] Sixun Jiang,[b] Tingting Han,[a] Shuai Wu,[a] Yukui Tian,[ac] and Feng Wang*[b]*

[a] Institutes of Physical Science and Information Technology, Anhui University, Hefei, Anhui 230601, China. E-mail: tianyk@ahu.edu.cn

[b] Key Laboratory of Soft Matter Chemistry, Hefei National Laboratory for Physical Science at the Microscale, Department of Polymer Science and Engineering, University of Science and Technology of China, Hefei, Anhui 230026, China. E-mail: drfwang@ustc.edu.cn

[c] School of Materials Science and Engineering, Anhui University, Hefei 230601, China.

Table of Content

1. Materials and Methods

Reagents. Silver tetrafluoroborate ($AgBF_4$), potassium tetrachloroplatinate(II) (K_2PtCl_4), copper(I) iodide (CuI), 2,6-diacetylpyridine, pivalic acid, (1*R*)-(–)-myrtenal were reagent grade and used as received. Compounds **2**[S1], **7**[S2], and **5**[S3] were synthesized according to the previously reported procedures. Other reagents and solvents were employed as purchased.

Experimental apparatus. ^{1}H NMR spectra was collected on a Bruker Ascend™ 400MHz spectrometer with TMS as the internal standard. ^{13}C NMR spectra were recorded on a Bruker Ascend™ 400 MHz spectrometer at 100 MHz. Time-of-flight mass spectra (TOF−MS) were obtained on matrix-assisted laser desorption ionization-time of flight (autoflex speed TOF/TOF, Bruker). UV−Vis spectra were recorded on a UV-1800 Shimadzu spectrometer. HPLC was performed on an Agilent system (1260 Infinity II) equipped with a DAD detector. Fluorescent spectra were recorded on a Fluoromax-4 spectrofluorometer (Horiba Scientific). Circular dichroism (CD) measurements were performed on a Jasco J-1500 circular dichroism spectrometer, equipped with a PFD-425S/15 Peltier-type temperature controller.

DFT and TD-DFT calculations. All of the optimized geometries were optimized *via* Gaussian 09 (revision D.01) software package.[S4]

*Method for determination of self-association constant of **1** by UV–Vis measurements.* To acquire the detailed thermodynamic parameters for the temperature-dependent self-assembly process, the obtained UV–Vis spectra data were normalized between 0 and 1 using the following **Eq. S1**. The normalized UV–Vis heating curve is further fitted by the monomer–dimer mathematical model,[S5] as depicted by **Eq. S2**.

$$\alpha_{agg}(T) = \frac{A(T) - A_{mon}}{A_{agg} - A_{mon}} \quad \textbf{(Eq. S1)}$$

$$\alpha_{agg}(T) = \frac{1}{1 + exp\left[\frac{T - T_m}{T^*}\right]}$$ **(Eq. S2)**

In these equations, $A_{(T)}$ is UV–Vis spectra absorbance date at a given temperature. $A_{(mon)}$ is the UV–Vis absorbance date at high temperature or good solvent corresponding to the monomeric state, while $A_{(agg)}$ is UV–Vis spectra absorbance date at a given low temperature or poor solvent corresponding to the self-complexed dimeric state. T_m is the temperature at which the fraction of the self-complexed dimer (α_{agg}) is 0.5. T^* value is obtained by fitting equation **(Eq. S2)** to the experimental data. Depending on T_m at various concentration, the dimerization binding constant (K_{dim}) can be calculated.

Method for determination of the $\mathbf{1}_2$ *dimeric self-complexion constant by* ^{1}*H NMR measurements.* Depending on ^{1}H NMR dilution experiments, the dimerization binding constant can be calculated. In particular, it is based on the concentration-dependent proton resonance versus concentration, according to the following equation:[S6]

$$\delta_{obs} = \delta_m + (\delta_{mc} - \delta_m) \times f_c = \delta_m + (\delta_{mc} - \delta_m) \times \frac{\sqrt{1 + 8K_a[M]_0} + 1}{\sqrt{1 + 8K_a[M]_0} - 1}$$

(**Eq. S3**)

In particular, δ_{obs}, δ_m, and δ_c are the observed, monomeric (at infinite diluted state) and dimeric (at infinite concentrated state) chemical shifts, respectively. $[M]_0$ is the monomer concentration.

Method for determination of the host/guest binding constants. The non-covalent binding constants (K_a) of host/guest complexes **1**⊃**2** and **3** **2** were determined *via* UV–Vis titration experiments. The collected absorbance data (A) at the specific wavelength were probed *versus* concentration of the titrating species (C_A). A global fitting analysis was adopted *via* the Matlab–based global analysis program (*fitting program*) written by P. Thordarson *et al.* (*Supramol. Chem.* **2012**, *24*, 585; *Chem. Soc. Rev.* **2011**, *40*, 1305). [S7]

*Method for determination of the "real" association constant of **1**⊃**2***. The experimental result provided the "apparent" binding constant for complex **1**⊃**2**, since the non-covalent complexation between metallotweezer **1** (A) and guest **2** (B) is governed by three equilibria:

$2A \leftrightharpoons A_2$ (**Eq. S5**)

$2B + A_2 \leftrightharpoons 2AB$ (**Eq. S6**)

$A + B \leftrightharpoons AB$ (**Eq. S7**)

where A, A_2, B and AB represent free **1**, self-complexation $\mathbf{1}_2$, free **2** and complex **1**⊃**2**, respectively. The equilibrium constants in this system are defined in the following equation:

$$K_{dim} = [A_2]/[A]^2 \quad \textbf{(Eq. S8)}$$

$$K_d = [AB]^2/([A_2] \times [B]^2) \quad \textbf{(Eq. S9)}$$

$$K_a = [AB]^2/([A_2] \times [AB]^2) \quad \textbf{(Eq. S10)}$$

where K_{dim}, K_d and K_a are the dimerization constant of A, the disproportionation constant of B with A_2 (the "apparent" binding constant), and the "real" association constant of A and B, respectively. The K_a value is determined according to **Eq. S11**:[S8]

$$K_a = (K_{dim} \times K_d)^{1/2} \quad \textbf{(Eq. S11)}$$

*2. Synthetic routes to compounds **1** and **3***

The synthetic routes toward the targeted compounds **1** and **3** are quite straightforward (Scheme S1). The key intermediate **5** was obtained *via* coordination between the chiral "pineno"-fused 2,2′:6′,2″-terpyridine **6** and $Pt(DMSO)_2Cl_2$. It further underwent CuI-catalyzed Pt(II)–acetylene coupling reaction with compounds **7** and **4** to provide the targeted compounds **1** and **3**, respectively. The structures for **1** and **3** were validated by means of NMR and MALDI-TOF-MS experiments (Figures S7–S11).

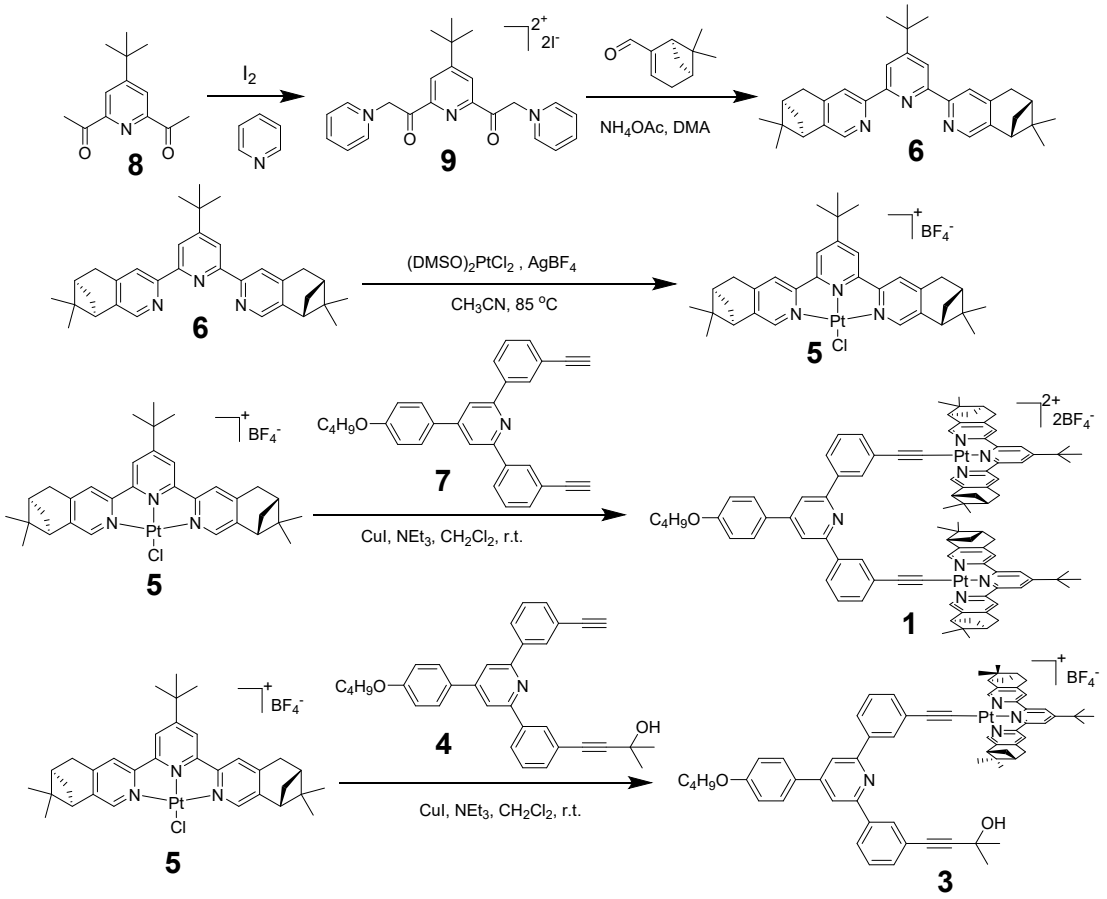

Scheme S1. Synthetic routes to compounds **1** and **3**.

*2.1 Synthesis of compound **6***

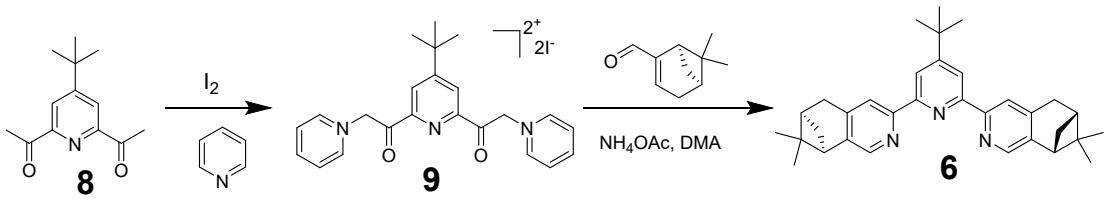

To a solution of compound **8** (23.0 mmol, 5.00 g) in pyridine (30 mL) was added a solution of iodine (46.0 mmol, 11.7 g) in pyridine (30 mL). The mixture was heated at 110 °C for 3 h. Upon cooling, the dull yellow solid was filtered and washed with cold ethanol to afford **9** as a brown solid (11.5 g, 80%), which were used for the next step without further purification. To a solution of compound **9** (2.00 g, 3.18 mmol) in formamide (30 mL) were added ammonium acetate (1.00 g, 13.0 mmol) and (1*R*)-(−)-myrtenal (1.00 g, 6.70 mmol) under nitrogen. The reaction mixture was stirred at 80 ℃ overnight under nitrogen atmosphere. After the reaction was complete, the solvent was evaporated under reduced pressure, and the residue was purified by flash column chromatography (alumina, CH_2Cl_2/PE,1 : 1, *v*/*v* as the eluent) to afford **6** as a white solid (0.65 g, 43%).^{1}H NMR (400 MHz, $CDCl_3$, 298 K, Figure S1) δ (ppm): 8.40 (d, J = 8.1 Hz, 4H), 8.24 (d, J = 0.7 Hz, 2H), 3.13 (s, 4H), 2.89 (t, J = 5.4 Hz, 2H), 2.77 – 2.70 (m, 2H), 2.35 (dt, J = 5.8, 3.0 Hz, 2H), 1.59 (s, 7H), 1.47 – 1.45 (m, 9H), 1.26 (s, 2H), 0.68 (s, 6H). ^{13}C NMR (101 MHz, $CDCl_3$, 298 K, Figure S2) δ: 161.9, 155.8, 155.1, 145.4, 145.2, 142.7, 117.5, 44.6, 40.2, 39.3, 35.3, 33.1, 31.9, 30.8, 26.1, 21.4. ESI *m*/*z*: $[M–BF_4]^+$, 478.3220 (Figure S3).

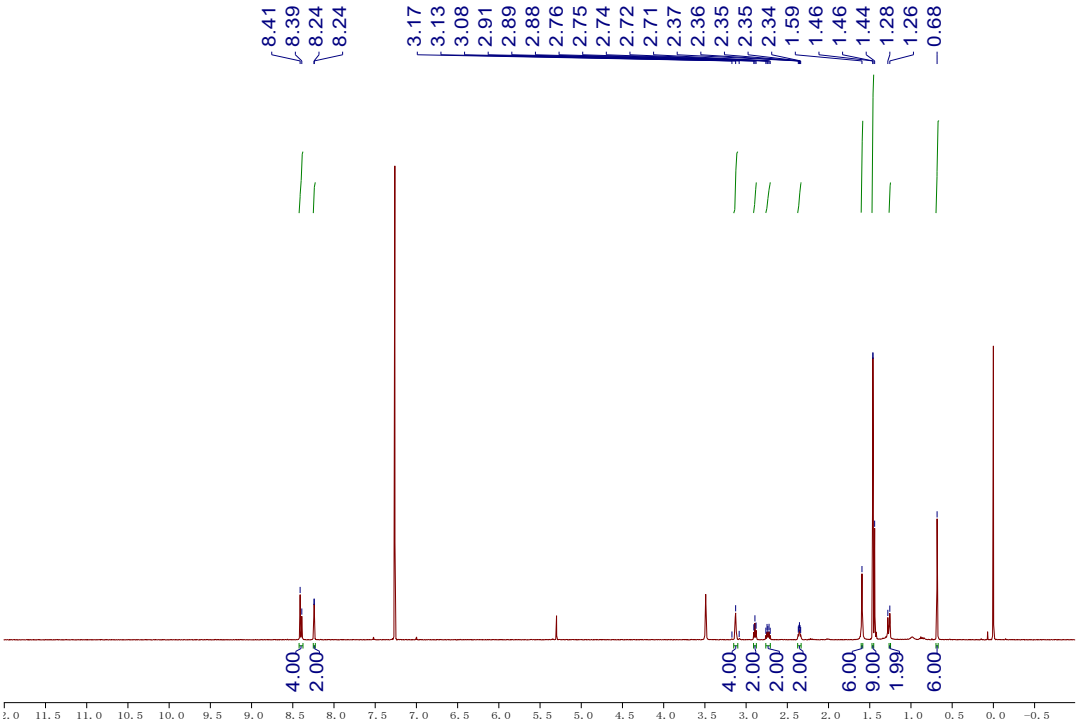

Figure S1. ^{1}H NMR spectrum (400MHz, $CDCl_3$, 298K) of compound **6**.

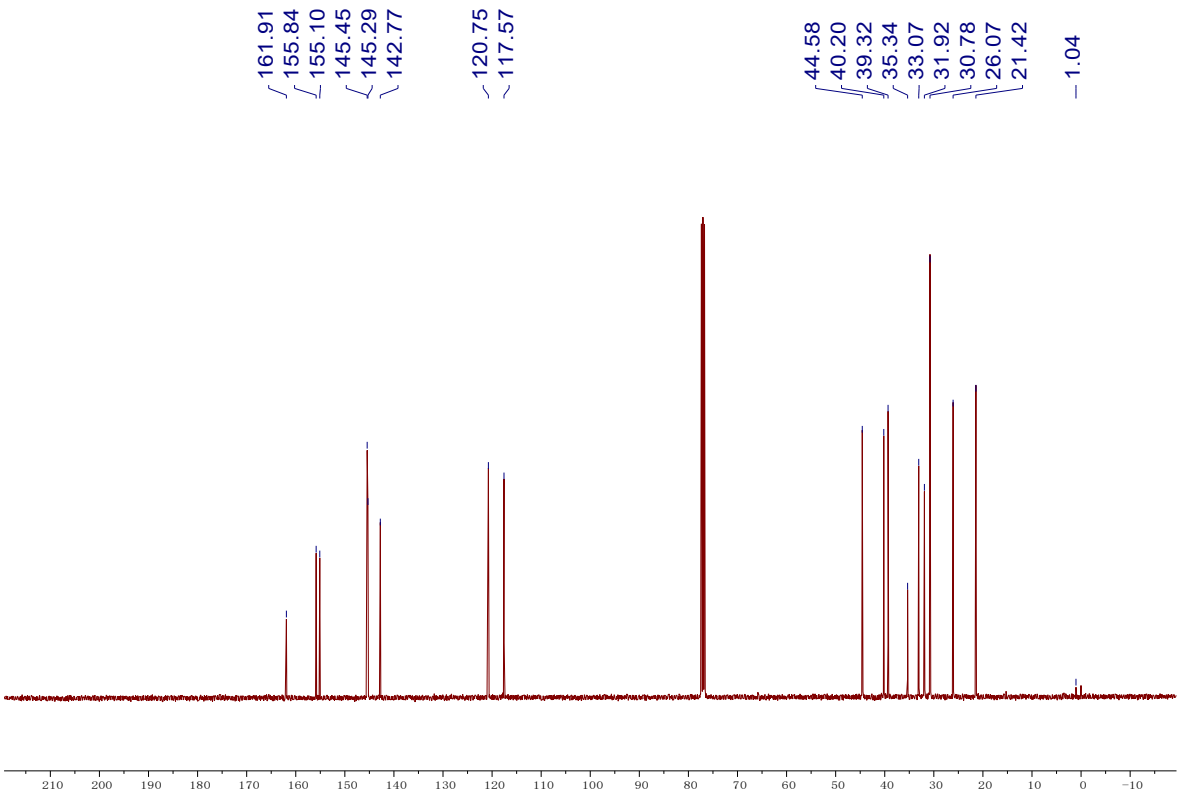

Figure S2. ^{13}C NMR spectrum (400MHz, $CDCl_3$, 298K) of compound **6**.

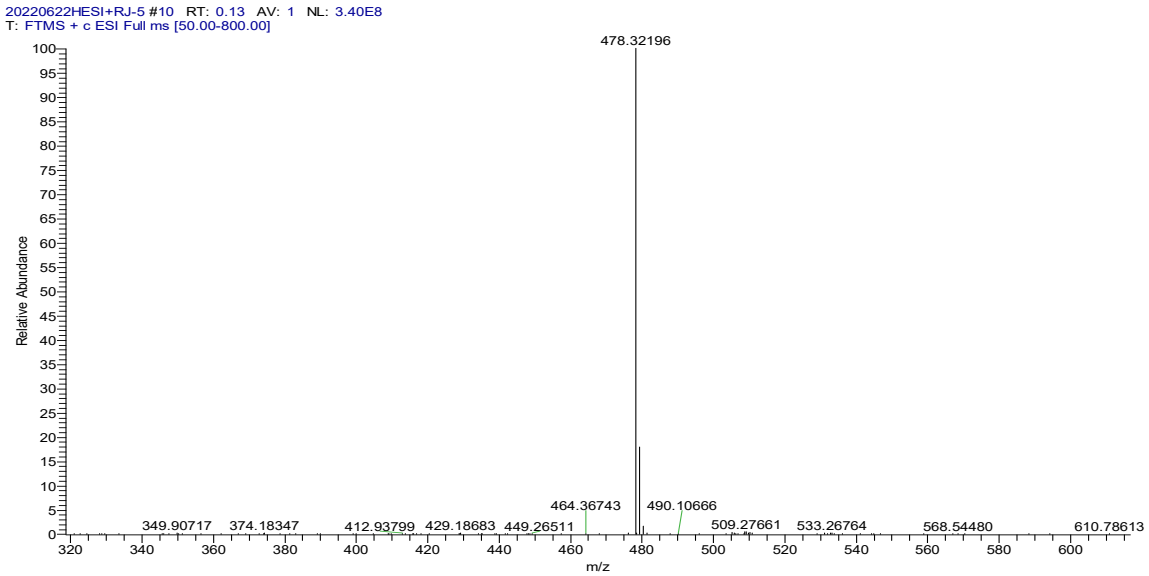

Figure S3. ESI spectrum of compound **6**.

2.2 Synthesis of compound ***5***

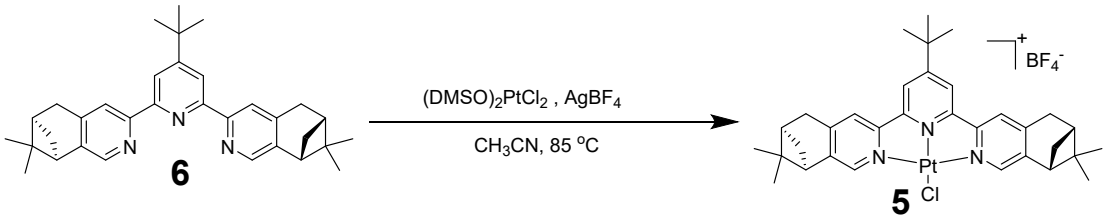

$Pt(DMSO)_2Cl_2$ (302 mg, 0.78 mmol) and $AgBF_4$ (152 mg, 0.86 mmol) in CH_3CN (15 mL) were placed in a round bottomed flask and refluxed for 24 hours. The mixture was then filtered, and compound **6** (340 mg, 0.71 mmol) was added. The resulting mixture was refluxed for another 24 hours. The solvent was evaporated under reduced pressure and the residue was purified by flash column chromatography (alumina, CH_3OH/CH_2Cl_2, 1:100, *v*/*v* as the eluent) afford compound **5** as a yellow solid (173mg, 66%). ^{1}H NMR (400 MHz, $CDCl_3$, 298 K, Figure S4) δ (ppm): 8.60 (s, 2H), 8.30 (s, 2H), 8.28 (s, 2H), 3.34 (s, 4H), 3.00 (t, J = 5.5 Hz, 2H), 2.82 – 2.76 (m, 2H), 2.44 – 2.39 (m, 3H), 1.59 (s, 9H), 1.46 (s, 6H), 1.26 (s, 2H), 0.70 (s, 6H). ^{13}C NMR (101 MHz, $CDCl_3$, 298 K, Figure S5) δ: 168.3, 156.3, 154.6, 153.1, 148.7, 146.8, 125.3, 120.7, 45.1, 42.0, 39.4, 38.9, 37.3, 33.6, 30.9, 30.2, 29.7, 27.0, 25.6, 24.9, 21.5. ESI *m*/*z*: $[M-BF_4]^+$, 707.2458 (Figure S6).

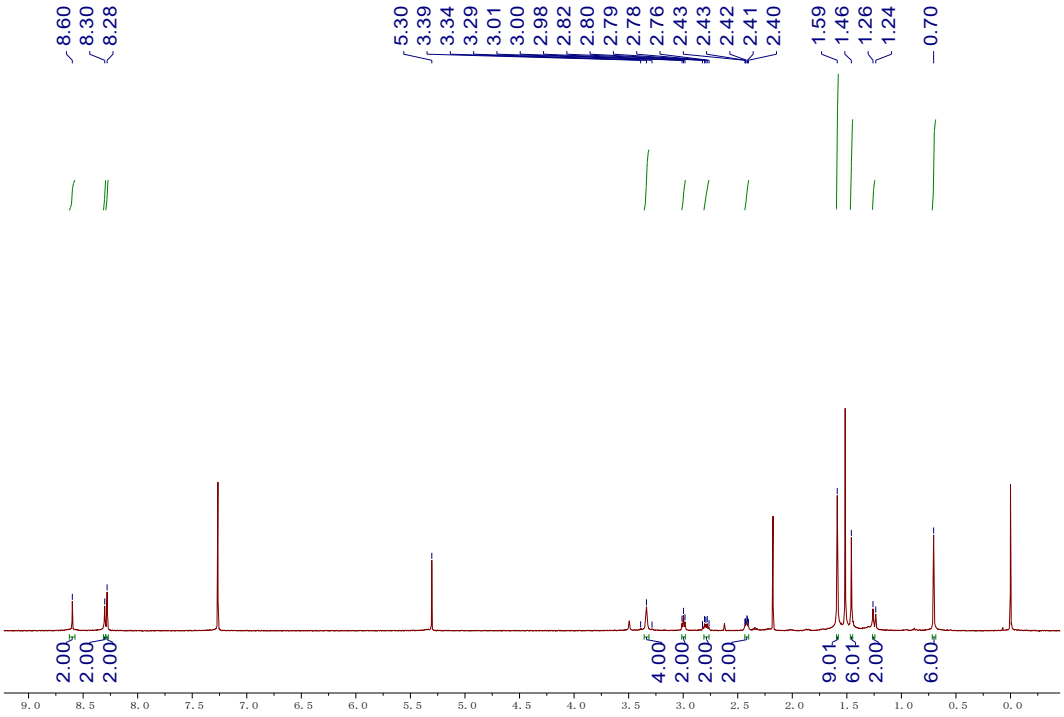

Figure S4. ^{1}H NMR spectrum (400MHz, $CDCl_3$, 298K) of compound **5**.

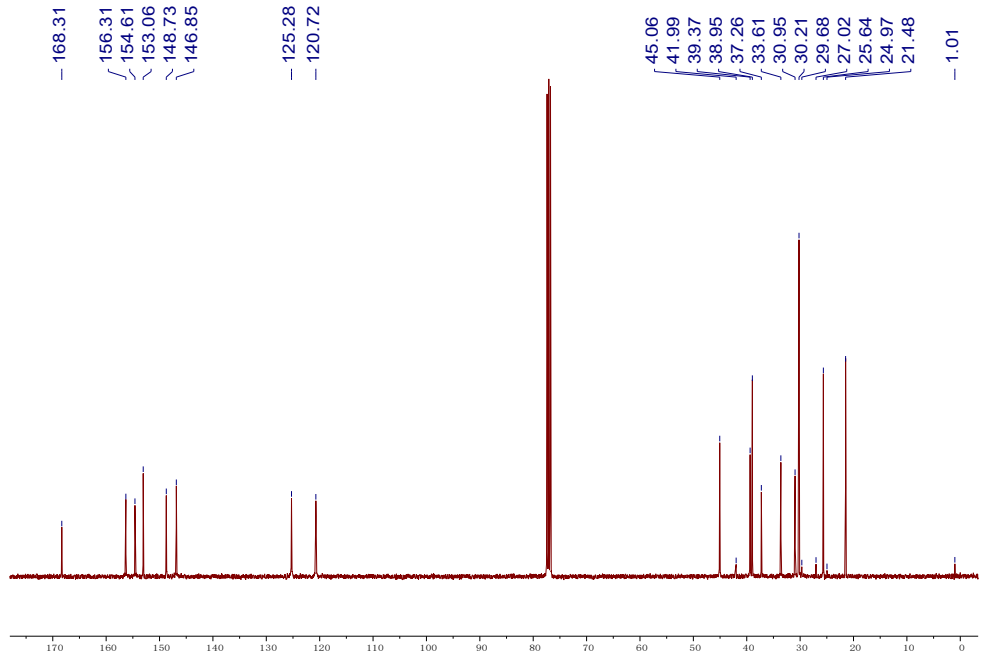

Figure S5. ^{13}C NMR spectrum (400MHz, $CDCl_3$, 298K) of compound **5**.

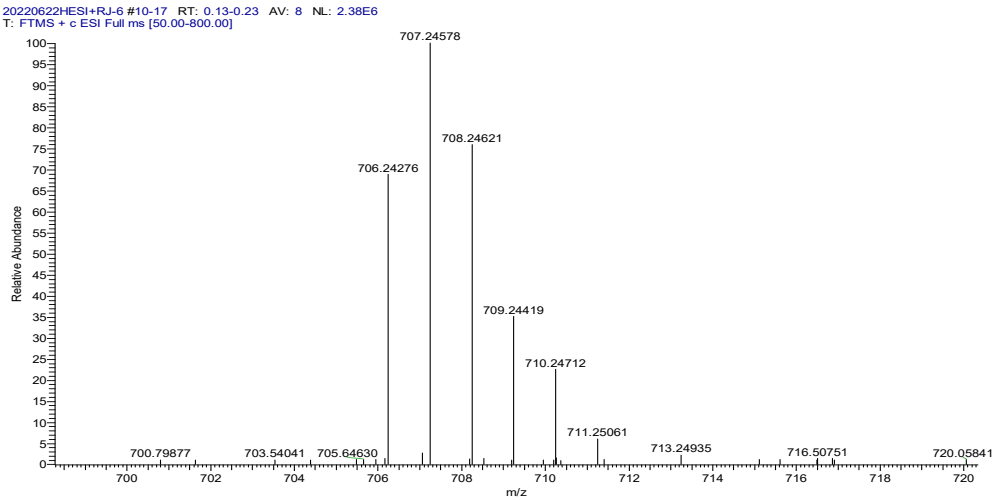

Figure S6. MALDI-TOF-MS spectrum of compound **5**.

*2.3 Synthesis of compound **1***

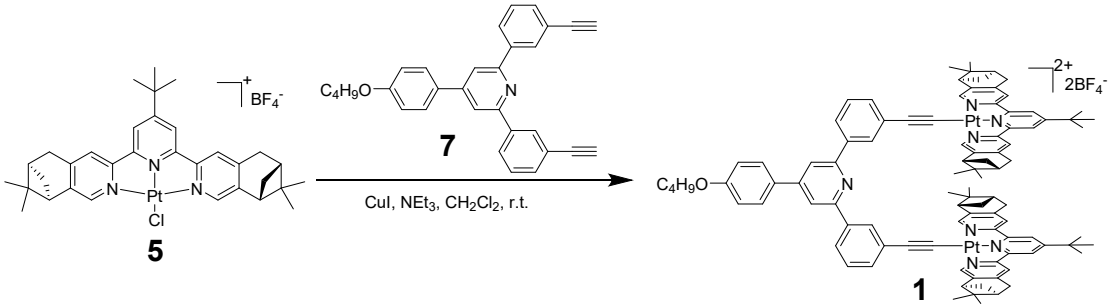

Compound **7** (50.0 mg, 1.17 mmol), Compound **5** (199 mg, 2.46 mmol), CuI (30.0 mg, 0.15 mmol) and NEt_3 (3 mL) in 20 mL of CH_2Cl_2 were stirred at room temperature for 48 hours under nitrogen atmosphere. The mixture was evaporated under reduced pressure and the residue was purified by column chromatography (alumina, CH_3OH/CH_2Cl_2, 100 : 1 *v*/*v* as the eluent) to afford metallotweezer **1** as an orange solid (143 mg, 63%).^{1}H NMR (400 MHz, $CDCl_3$, 298 K, Figure S7) δ (ppm): 8.77 (s, 3H), 8.53 (s, 4H), 8.39 (d, J = 13.2 Hz, 6H), 8.06 (d, J = 8.0 Hz, 2H), 7.91 (s, 2H), 7.71 (d, J = 8.7 Hz, 2H), 7.62 (d, J = 7.7 Hz, 2H), 7.48 (t, J = 7.7 Hz, 2H), 7.05 (d, J = 8.8 Hz, 2H), 4.04 (t, J = 6.5 Hz, 2H), 3.31 (s, 8H), 2.94 (t, J = 5.3 Hz, 4H), 2.75 – 2.66 (m, 4H), 2.40 – 2.31 (m, 4H), 1.81 (s, 4H), 1.48 (s, 19H), 1.37 (s, 13H), 1.23 (s, 4H), 1.00 (t, J = 7.4 Hz, 3H), 0.67 (s, 12H). ^{13}C NMR (101 MHz, $CDCl_3$, 298 K, Figure S8) δ: 167.2, 159.2, 156.3, 155.6, 153.2, 151.3, 148.9, 148.7, 148.0, 138.7, 131.5, 129.7, 129.4, 127.5, 127.2, 126.1, 124.6, 124.5, 119.6, 115.8, 114.1, 103.6, 97.3, 69.5, 66.9, 43.9, 38.4, 37.9, 36.5, 32.7, 30.3, 30.1, 29.6, 24.6, 20.5, 18.24. MALDI−TOF−MS *m/z*:

$[M\text{-}BF_4]^+$, 1856.7603.

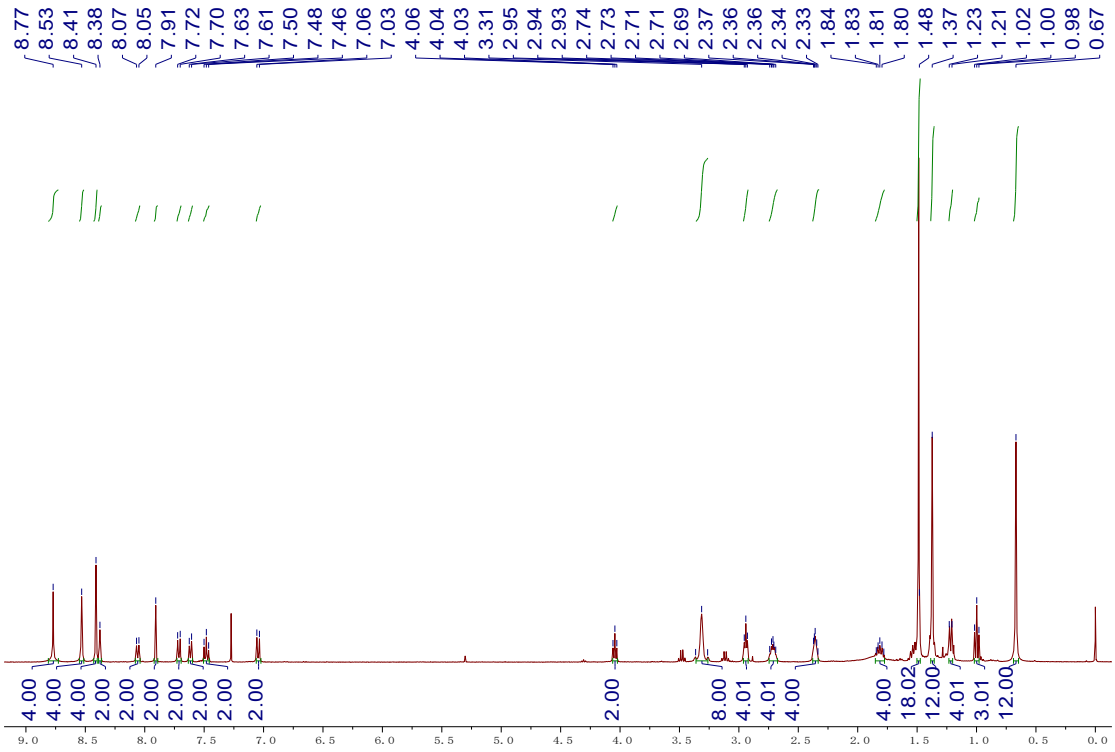

Figure S7. ^{1}H NMR spectrum (400MHz, $CDCl_3$, 298K) of compound **1**.

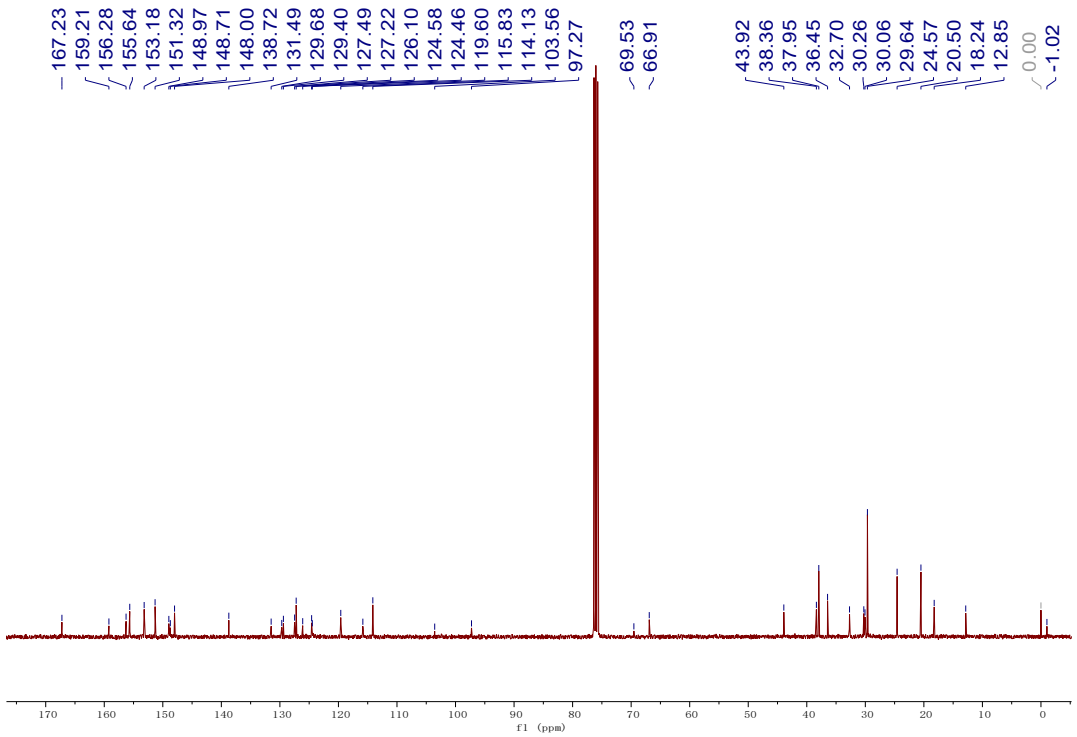

Figure S8. ^{13}C NMR spectrum (400MHz, $CDCl_3$, 298K) of compound **1**.

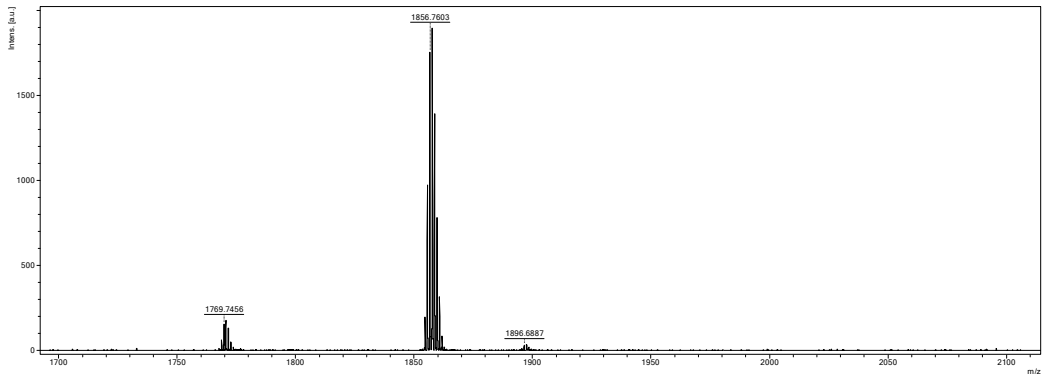

Figure S9. MALDI-TOF-MS spectrum of compound **1**.

*2.4 Synthesis of compound **3***

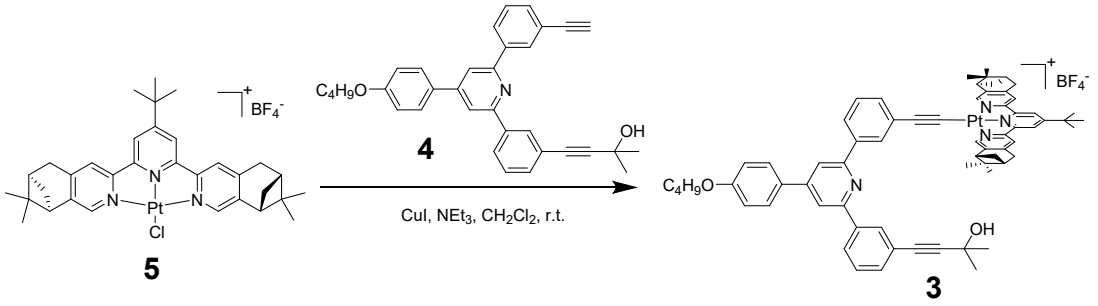

Compounds **4** (50.0 mg, 1.17 mmol), **5** (89.0 mg, 1.12 mmol), CuI (30.0 mg, 0.15 mmol) and NEt_3 (3 mL) in 20 mL of CH_2Cl_2 were stirred at room temperature for 48 hours under nitrogen atmosphere. The mixture was evaporated under reduced pressure and the residue was purified by column chromatography (alumina, CH_3OH/CH_2Cl_2, 100 : 1 *v*/*v* as the eluent) to afford **3** as an orange solid (88.0 mg, 60%).^{1}H NMR (400 MHz, $CDCl_3$, 298 K, Figure S10) δ (ppm): 8.80 (s, 2H), 8.72 (s, 2H), 8.53 (s, 2H), 8.31 (t, J = 1.8 Hz, 1H), 8.20 – 8.17 (m, 2H), 8.11 (d, J = 7.9 Hz, 1H), 7.91 (s, 1H), 7.86 (s, 1H), 7.71 (d, J = 8.7 Hz, 2H), 7.62 (d, J = 8.3 Hz, 1H), 7.54 – 7.42 (m, 4H), 7.05 (d, J = 8.9 Hz, 2H), 4.05 (t, J = 6.6 Hz, 2H), 3.38 – 3.31 (m, 4H), 2.98 (t, J = 5.4 Hz, 2H), 2.79 – 2.70 (m, 3H), 2.43 – 2.36 (m, 2H), 1.86 – 1.78 (m, 3H), 1.60 (s, 9H), 1.40 (s, 6H), 1.25 (s, 7H), 1.00 (t, J = 7.4 Hz, 4H), 0.88 (t, J = 6.8 Hz, 3H), 0.70 (s, 6H). We failed to acquire the ^{13}C NMR spectrum of **3** due to its low solubility. MALDI−TOF−MS *m/z*: $[M\text{-}BF_4]^+$, 1156.4603 (Figure S11).

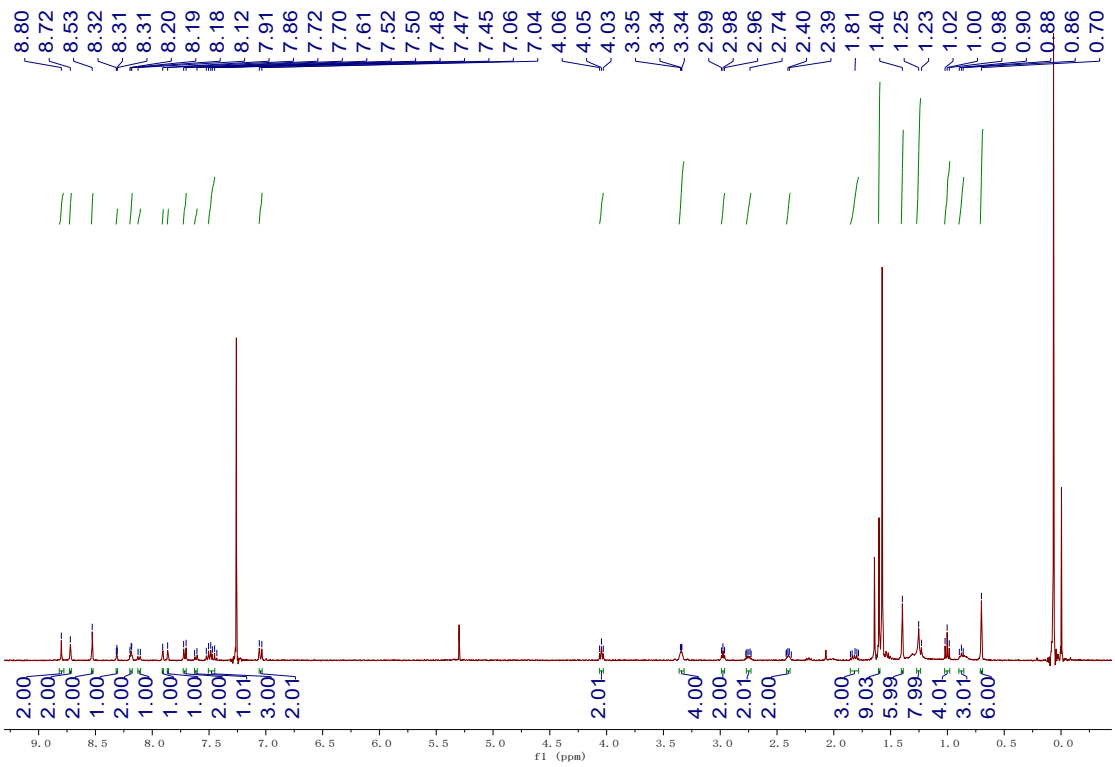

Figure S10. ^{1}H NMR spectrum (400MHz, $CDCl_3$, 298K) of compound **3**.

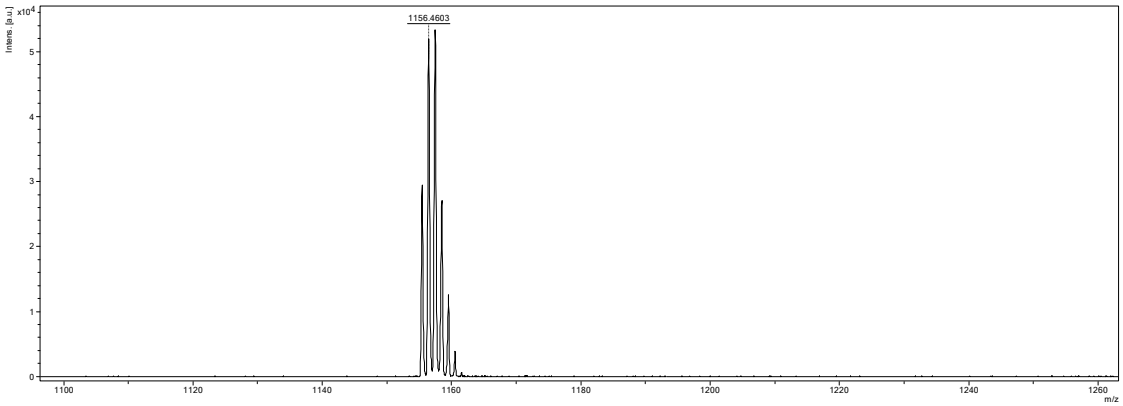

Figure S11. MALDI-TOF-MS spectrum of compound **3**.

3. *The dimeric self-complexation behaviors of **1***

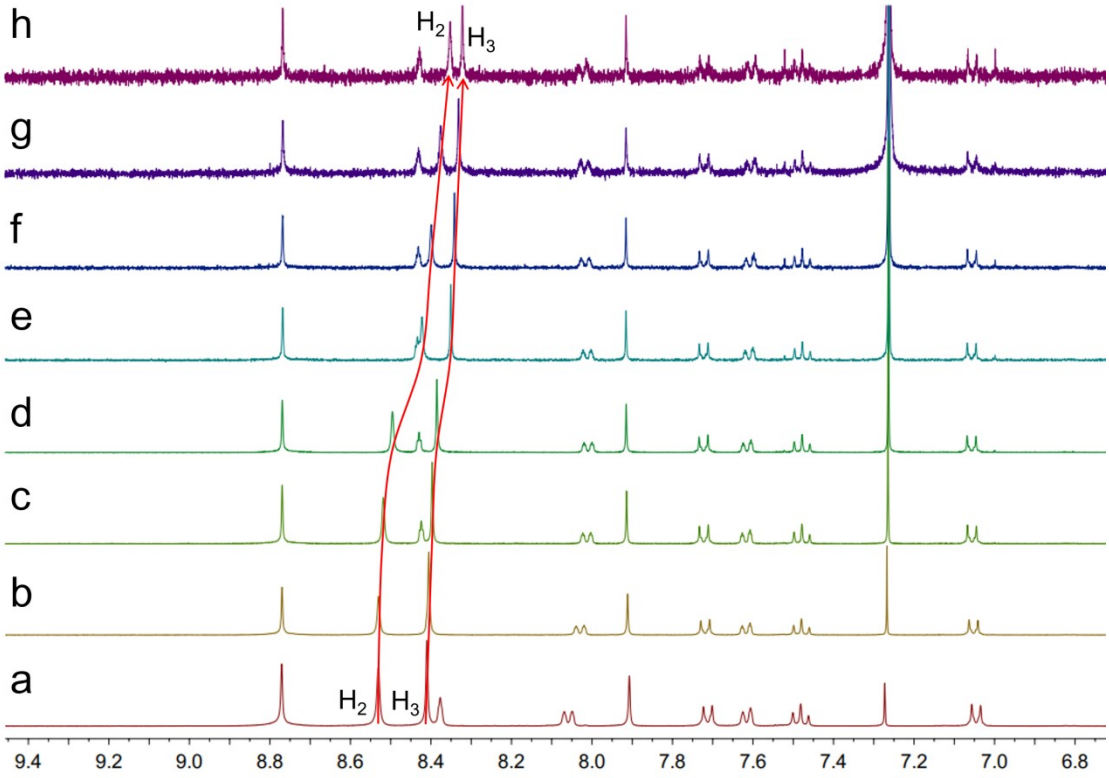

Figure S12. ^{1}H NMR spectra (400 MHz, $CDCl_3$, 298 K) of metallotweezer **1** at different monomer concentrations: a) 20.00 mM, b) 10.00 mM, c) 5.00 mM, d) 3.00 mM, e) 1.00 mM, f) 0.60 mM, g) 0.40 mM, h) 0.20 mM. Obvious chemical shift changes of H_2 and H_3 were observed for **1** upon varying its concentrations. It facilitates the acquirement of the dimeric K_{dim} value (see Figure S13).

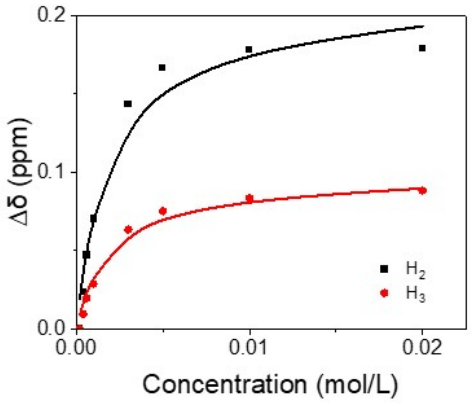

1 (mM)	H2 (ppm)	H3 (ppm)
20	8.5308	8.4102
10	8.5301	8.4055
5	8.5185	8.3971
3	8.4958	8.3853
1	8.4224	8.3507
0.6	8.3991	8.3415
0.4	8.3759	8.3313
0.2	8.3521	8.3219

Figure S13. Changes of chemical shifts (δ) of protons H_2 and H_3 on **1** upon varying its concentrations (in $CDCl_3$ at 298 K). The dimeric K_{dim} value for **1** was determined to be 5.34×10^2 M^{-1} ($\pm$ 34%), by fitting the collected δ data of protons of H_2 and H_3 on **1** in ^{1}H NMR titration experiments. The data values were fitted by Matlab–based global analysis program.

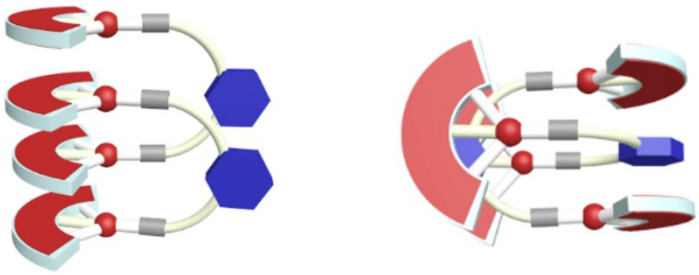

Quadruple π-stacks type Self-complementary type

Figure S14. Graphic representation of quadruple π-stacks and self-complementary type complexation structures for molecular tweezers. It commonly contains two modes for self-aggregation of molecular tweezers, namely quadruple π-stacks, and self-complementary dimers complexation structures. For the latter complexation modes, the spacer on molecular tweezer should be planar and electrically complementary to the pincer units, as exemplified by the bis-methyl amide functionalized pyridine and terpyridine unit reported in the previous literatures.[S9] In the current molecular tweezer **1**, the diphenylpyridine spacer is non-planar (possessing a 17.5° deviation from coplanar geometry as reported in a structurally similar tweezer),[S10] and thereby fails to be encapsulated into the cavity of molecular tweezer. Accordingly, it excludes the possibilities of the latter complexation mode.

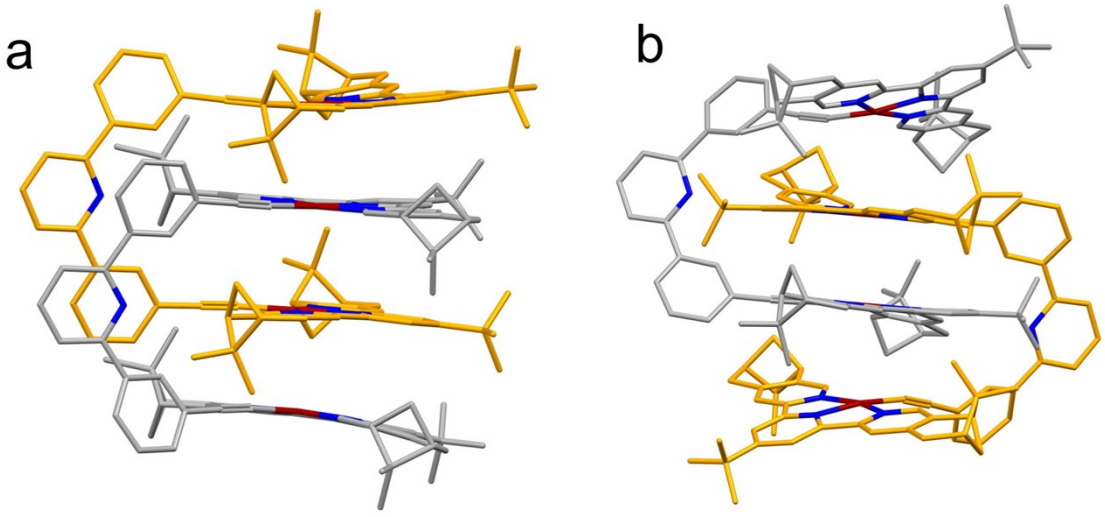

Head-to-head binding model

-7971.865426 a.u.

Head-to-tail binding model

-7971.863874 a.u.

Figure S15. Four complexation modes of $\mathbf{1}_2$ *via* DFT computation: a) head-to-head binding model; b) head-to-tail binding model. For the optimized geometries, the head-to-head binding mode features lower Gibbs free energy than that of the head-to-tail one (ΔE = 0.974 kcal/mol).

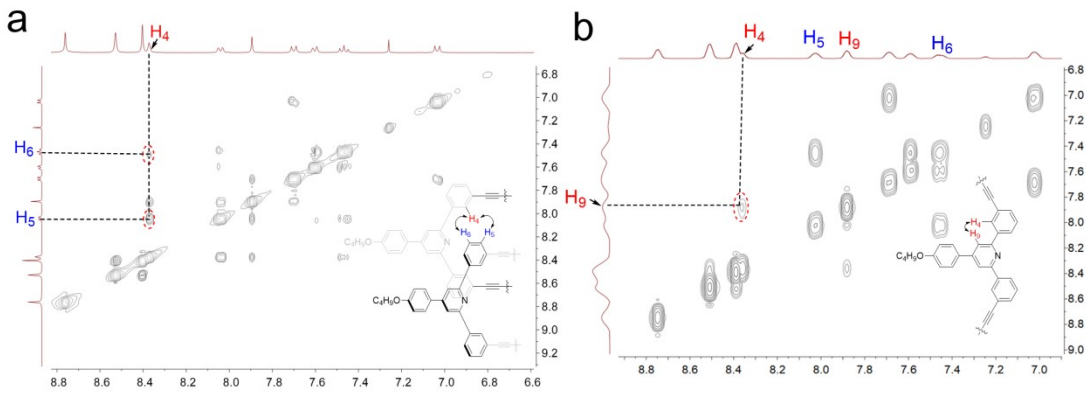

Figure S16. Partial a) ^{1}H–^{1}H ROESY and b) ^{1}H–^{1}H COSY spectrum (400 MHz, $CDCl_3$, 298 K) of $\mathbf{1}_2$. Strong correlations existed between protons H_4 and H_5/H_6 in ^{1}H–^{1}H ROESY, which were absent in ^{1}H–^{1}H COSY spectrum.

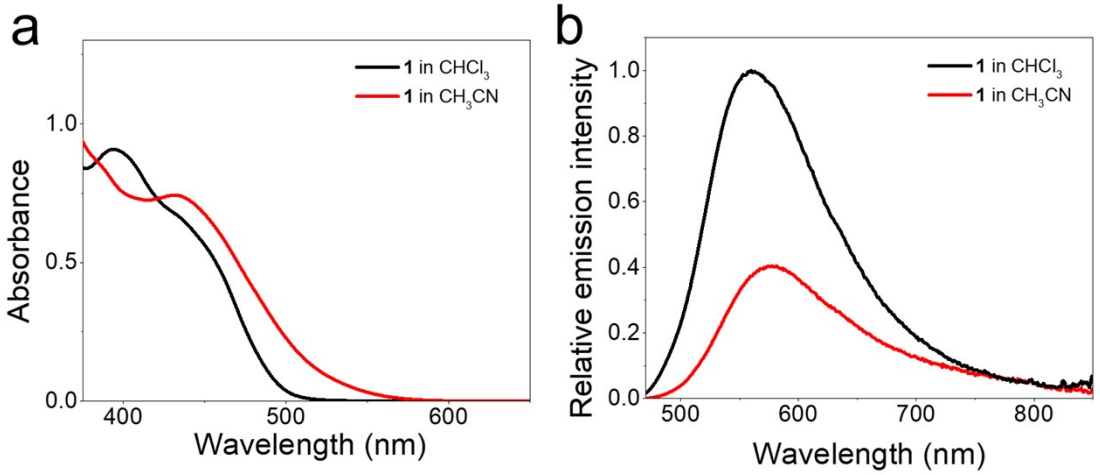

Figure S17. a) Absorption and b) emission spectra of **1** in CH_3CN and $CHCl_3$ at 298K [c = 1.00 × 10^{-4} M].

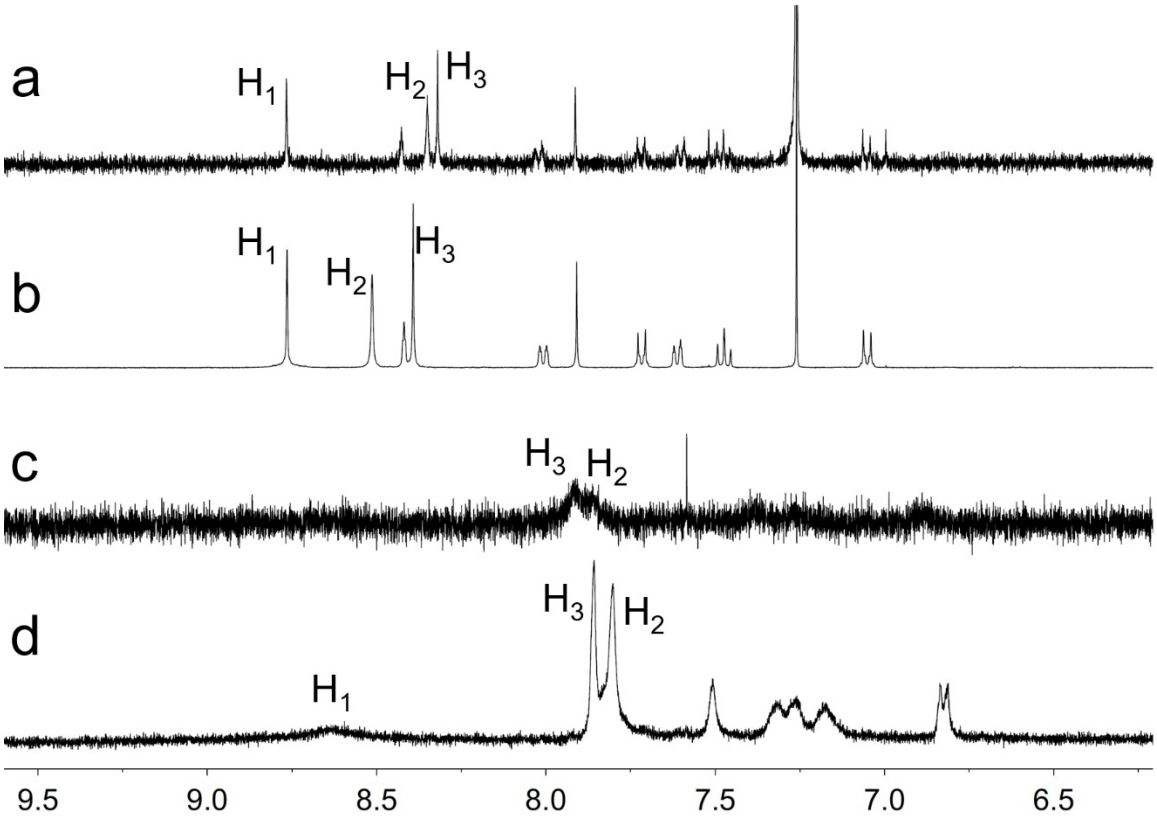

Figure 18. ^{1}H NMR spectra (400 MHz, 298K) of molecular tweezers **1** at different concentrations: a) 0.20 mM, and b) 5.00 mM in $CDCl_3$; c) 0.20 mM, and d) 5.00 mM, in CD_3CN.Such phenomenon indicate the strong binding affinity for $(\mathbf{1})_2$ and the binding constants could not be calculated by ^{1}H NMR concentration dependent experiments. In CD_3CN, the aromatic resonances became broadened compared to those in $CDCl_3$, while some of the peaks were merged into baseline. It suggests that the self-complexation structure $(\mathbf{1})_2$ existed even in the dilute solution. Hence, the binding constant in CD_3CN cannot be acquired by concentration-dependent ^{1}H NMR experiments.

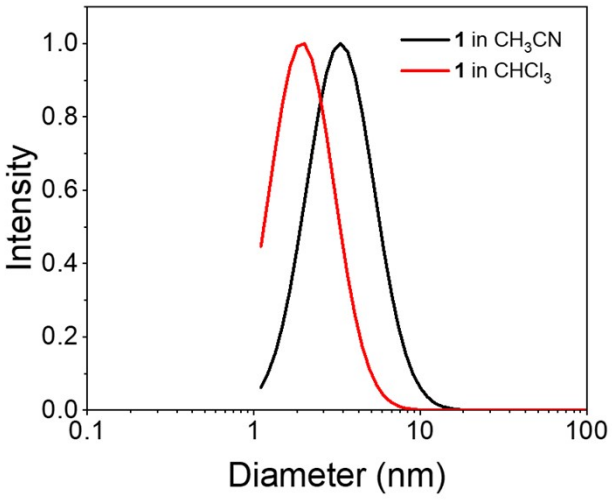

Figure S19. DLS measurements for **1** in CH_3CN and $CHCl_3$ (c = 1.00 × 10^{-4} M).

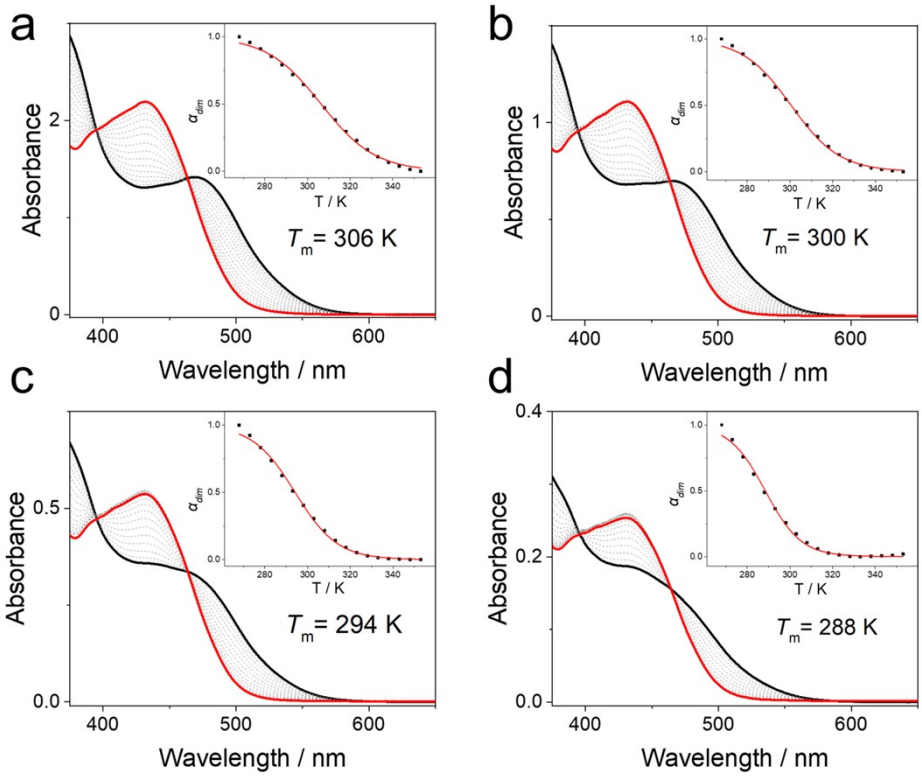

Figure S20. Temperature-dependent UV–Vis absorption spectra of **1** at different monomer concentrations: a) 0.2 Mm; b) 0.1 mM; c) 0.05 mM; d) 0.025 mM in CH_3CN. Inset: Fraction of α_{agg} of **1** monitored at 500 nm *versus* temperatures at different concentrations. The shoulder absorption band declined upon increasing the temperature to 353 K, and restored upon cooling to room temperature.

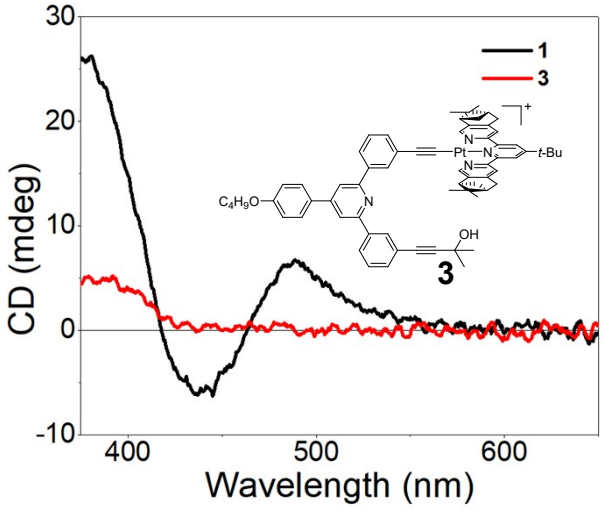

Figure S21. CD spectra of **1** and **3** at 298 K (c = 1.00 × 10^{-4} M in CH_3CN). Depending on circular dichroism (CD) experiments, a weak Cotton effect below 419 nm existed for the control compound **3** with the mono-nuclear Pt(II)(N^N^N) unit, supporting the origin of molecular chirality from the (1*R*)-pinene units.

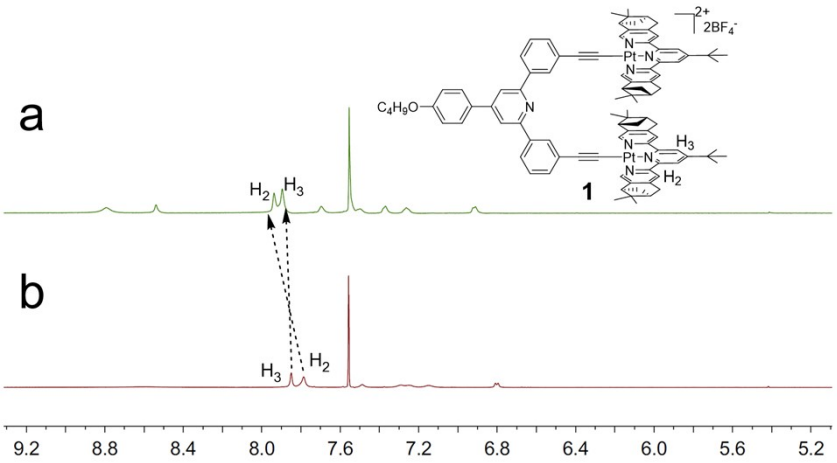

Figure S22. Partial ^{1}H NMR titration spectra (400 MHz, CD_3CN) at a) 353 K and b) 298 K. Upon increasing the temperature from 298 K to 353 K, the ^{1}H NMR resonances of $H_{2\text{-}3}$ exhibited a downfield shift from the self-complexed to the monomeric states of **1**.

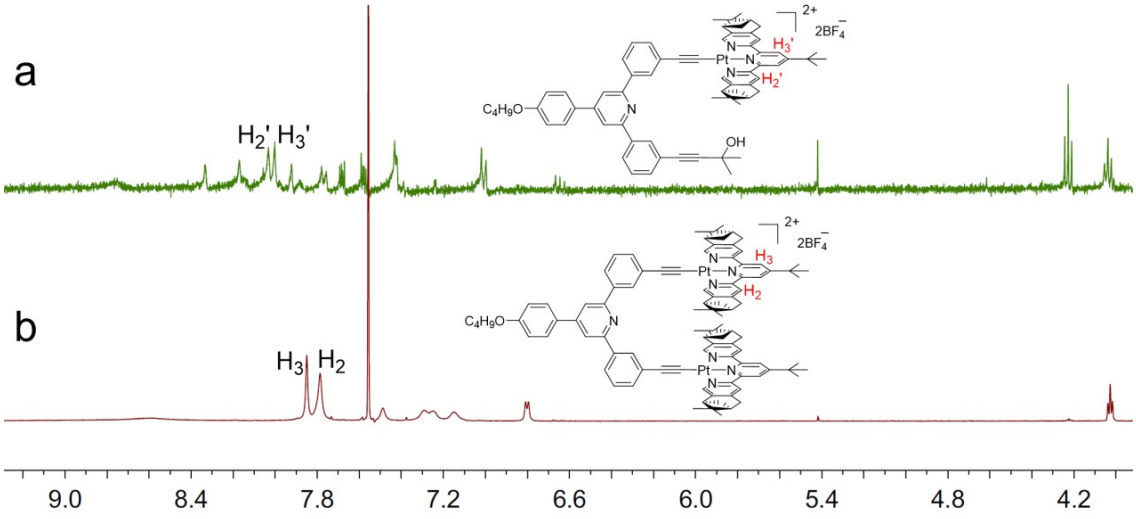

Figure S23. ^{1}H NMR titration spectra (400 MHz, CD_3CN, 298 K) for a) compound **3** and b) metallotweezer **1**. The terpyridine protons $H_{2\text{-}3}$ on **1** shifted upfield than the corresponding protons $H_{2'\text{-}3'}$ of **3**. It is ascribed to the formation of self-complexation structure with the de-shielding effect.

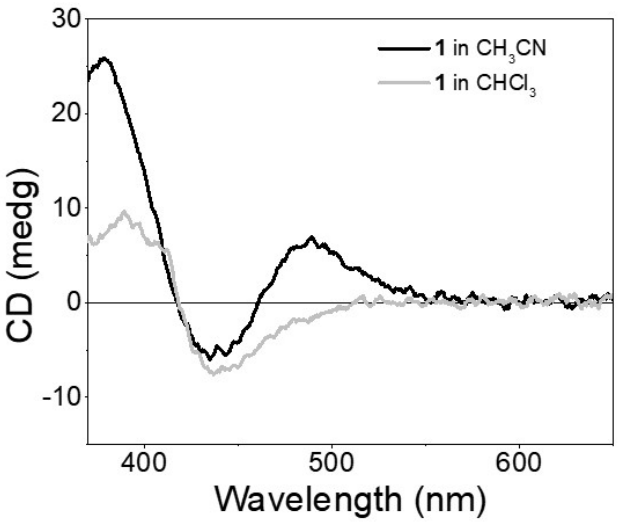

Figure S24. CD spectra of **1** in CH_3CN and $CHCl_3$ (c = 1.00 × 10^{-4} M at 298 K).

4. *Non-covalent metallotweezer/guest complexation behaviors*

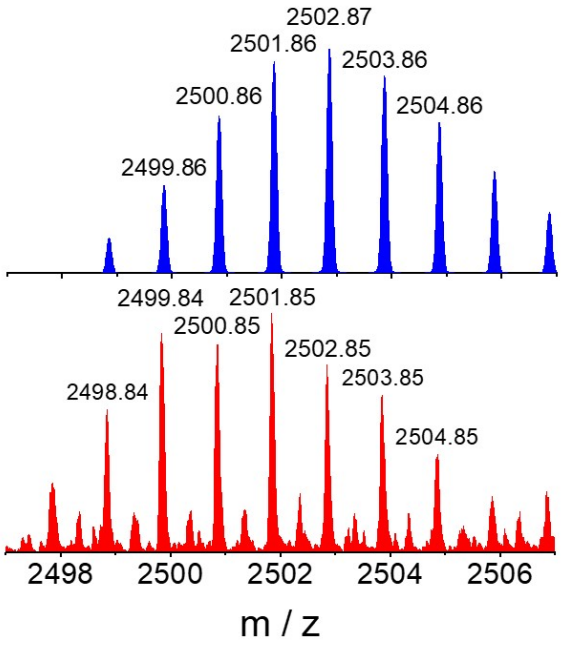

Figure S25. a) Absorption and b) emission spectra of **1** and complex **1**⊃**2** in CH_3CN at 0.05 mM. Inset: images of **1** and complex **1**⊃**2**.

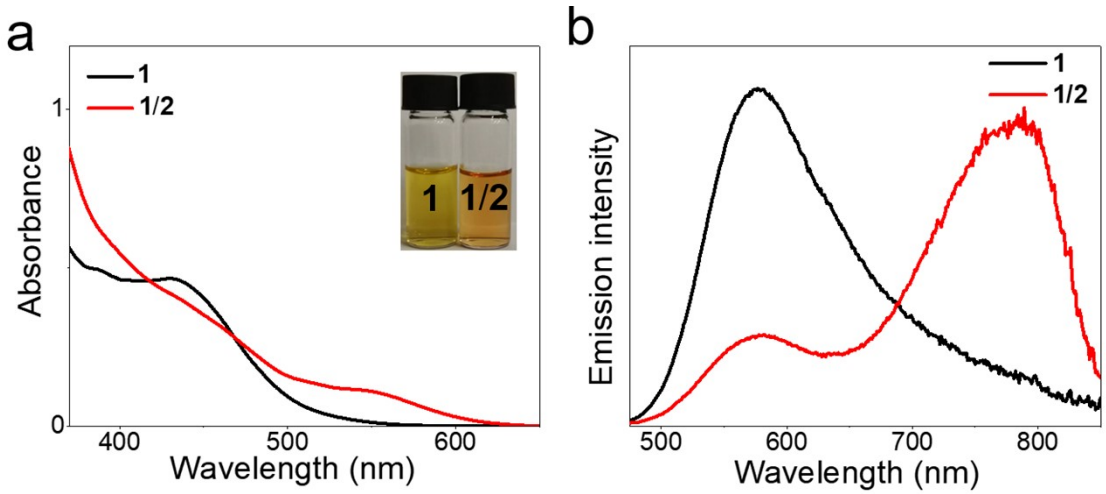

Figure S26. a) Absorption and b) emission spectra of **1** and complex **1**⊃**2** in CH_3CN at 0.05 mM. Inset: images of **1** and complex **1**⊃**2**.

a

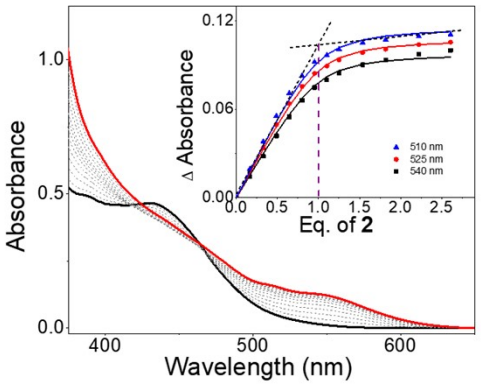

b

1 (mM)	2 (mM)	Abs. (510nm)	Abs. (525nm)	Abs. (540nm)
0.05	0	0.0619123	0.0342169	0.01839
	0.00826446	0.0762874	0.051609	0.03789
	0.0163934	0.0900704	0.0680434	0.05655
	0.0243902	0.103899	0.0839202	0.07389
	0.0322581	0.116835	0.0981173	0.0893
	0.04	0.127922	0.109761	0.10125
	0.047619	0.136684	0.118635	0.1104
	0.0551181	0.142063	0.123568	0.11524
	0.0625	0.14652	0.12786	0.1192
	0.0769231	0.152125	0.132717	0.1236
	0.0909091	0.155361	0.135063	0.12563
	0.111111	0.159322	0.138181	0.12792
	0.130435	0.161994	0.139834	0.12913

Figure S27. a) Changes of UV−Vis absorbance at 510 nm, 525 nm, and 540 nm upon addition of **2** (1.00 mM in CH_3CN) into **1** (0.05 mM in CH_3CN) at 298 K; b) Data values from the UV–Vis titration experiments (see Figure S26b) of **1**⊃**2** in CH_3CN at 298 K. Depending on the molar ratio plot, the binding stoichiometry between the tweezer receptor **1** and the guest **2** was 1 : 1. The solid lines are obtained *via* the Matlab–based global analysis program (fitting program). The K_d value of **1**⊃**2** is determined to be 3.75×10^5 M^{-1} (± 27%) in CH_3CN at 298 K. Accordingly, the K_a value of **1**⊃**2** is determined to be 6.96×10^4 M^{-1} (± 13%) in CH_3CN.

a

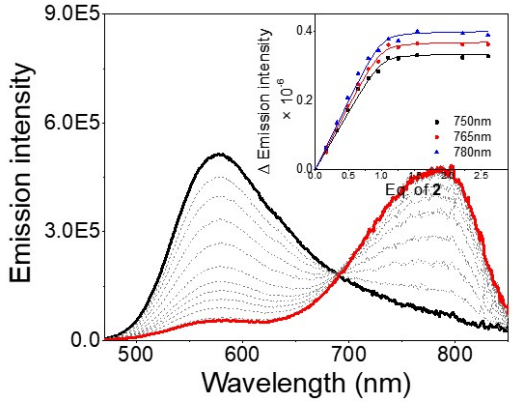

b

1 (mM)	2 (mM)	Intensity(750nm) × 10^{-6}	Intensity (765nm) × 10^{-6}	Intensity (780nm) × 10^{-6}
0.1	0	0	0	0
	0.01652	0.062092329	0.051055117	0.063853161
	0.0328	0.114101307	0.133885668	0.136148011
	0.0488	0.172209805	0.184320273	0.208301811
	0.0646	0.233176186	0.246421723	0.2780983
	0.08	0.264134457	0.291311792	0.321698069
	0.0952	0.284093587	0.312069795	0.344802821
	0.1102	0.32340768	0.360902559	0.376795138
	0.125	0.321497976	0.352792265	0.372924965
	0.1538	0.330787624	0.364202859	0.398419573
	0.222	0.324358028	0.362102984	0.394034246
	0.26	0.327912164	0.362100797	0.389232241

Figure S28. Emission spectra changes of **1** (0.1 mM) *via* the gradual titration of **2** (1.00 mM at 298 K) in CH_3CN. The solid lines are obtained *via* the Matlab–based global analysis program (fitting program). Accordingly, the K_d value of **1**⊃**2** is determined to be 2.21×10^6 M^{-1} (± 89%) in CH_3CN at 298 K. Accordingly, the K_a value of **1**⊃**2** is determined to be 1.69×10^5 (± 37%) in CH_3CN.

a

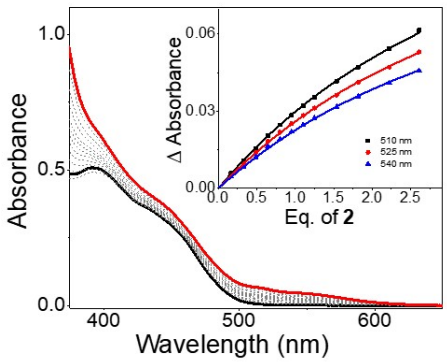

b

1 (mM)	2 (mM)	Abs. (510nm)	Abs. (525nm)	Abs. (540nm)
0.05	0	0.00745984	0.00253015	0.00140204
	0.00826446	0.0133308	0.00770728	0.00597404
	0.0163934	0.0182251	0.0120248	0.00973531
	0.0243902	0.023056	0.016526	0.0135343
	0.0322581	0.0279319	0.0209353	0.017726
	0.04	0.0321551	0.0243483	0.0205135
	0.047619	0.0358824	0.0277137	0.0234459
	0.0551181	0.0395477	0.0308573	0.026115
	0.0625	0.0429084	0.0337674	0.0287696
	0.0769231	0.0491226	0.0388166	0.0331566
	0.0909091	0.0546102	0.0437219	0.0371371
	0.111111	0.0619157	0.049688	0.0423657
	0.130435	0.0689838	0.0556343	0.0472103

Figure S29. a) Changes of UV−Vis absorbance at 510 nm, 525 nm, and 540 nm upon addition of **2** (1.00 mM in $CHCl_3$) into **1** (0.05 mM in $CHCl_3$) at 298 K; b) Data values from the UV–Vis titration experiments (see Figure S28b) of **1**⊃**2** in $CHCl_3$ at 298 K. The solid lines are obtained *via* the Matlab–based global analysis program (fitting program). The K_d value of **1**⊃**2** is determined to be 6.45×10^3 M^{-1} (± 6.5%) in $CHCl_3$. Accordingly, the K_a value of **1**⊃**2** is determined to be 1.85×10^3 M^{-1} (± 3.2%).

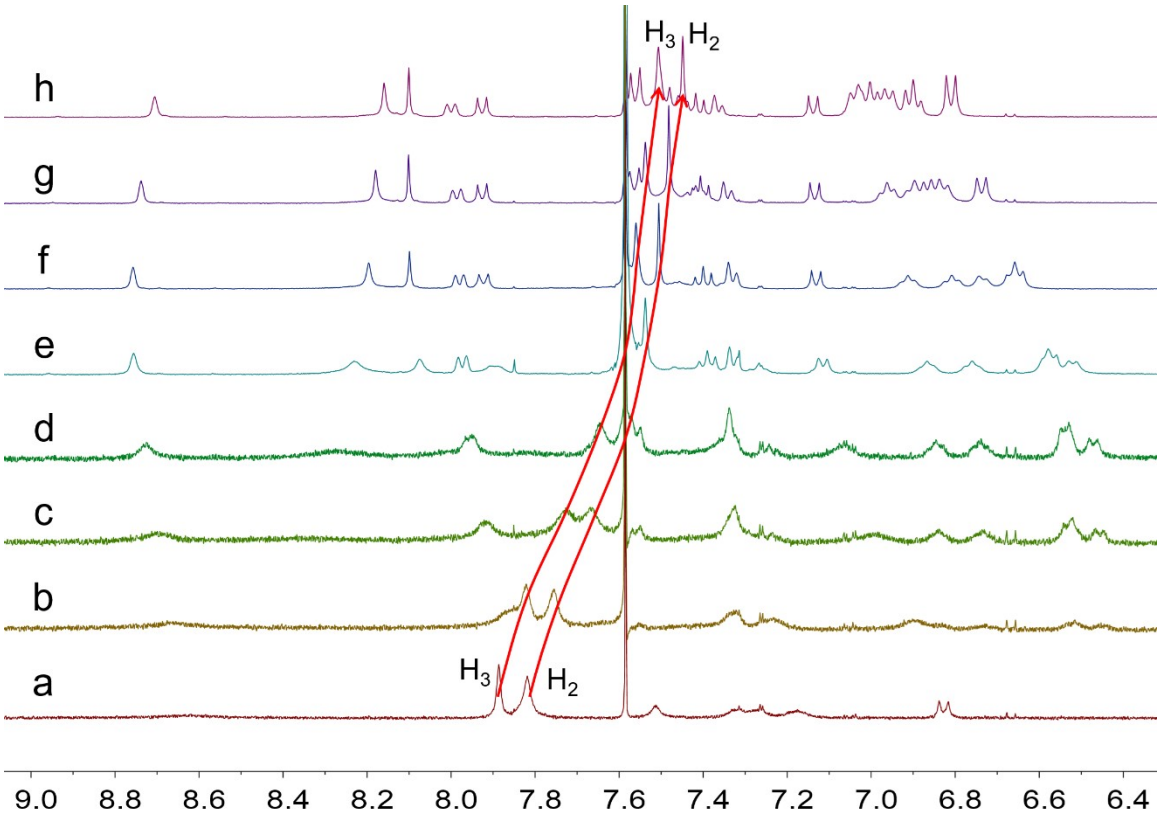

Figure S30. ^{1}H NMR spectra (400 MHz, CD_3CN, 298K) of complex **1**⊃**2** with different molar ratio of **2**: a) 0 eq.; b) 0.24 eq.; c) 0.48 eq.; d) 0.72 eq.; e) 0.96 eq.; f) 1.2 eq.; g) 1.68 eq.; h) 2.4 eq. Obvious chemical shift changes of H_2 and H_3 are observed for **1** upon addition of **2**, which is able to get the K_d value (Figure S29).

a

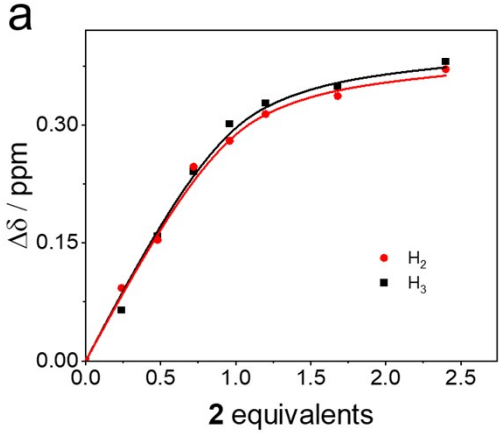

b

1 (mM)	2 (mM)	δ of H2(ppm)	δ of H3(ppm)
2.00	0	7.8466	7.9145
	0.48	7.7539	7.849
	0.96	7.6926	7.7543
	1.44	7.5997	7.6725
	1.92	7.5667	7.6134
	2.4	7.5328	7.587
	3.36	7.5098	7.5657
	4.8	7.4757	7.5338

Figure S31. a) Changes of chemical shifts (δ) of protons H_2, and H_3 on **1** upon addition of **2** into **1** (2 mM in CD_3CN) at 298 K; b) Data values from the ^1H NMR titration experiments (see Figure S30b) of **1**⊃**2** in CD_3CN at 298 K. The solid lines are obtained *via* a Matlab-based global analysis program (fitting program). The K_d value of **1**⊃**2** is determined to be 6.74×10^3 M^{-1} (± 63.4%) in CD_3CN. Accordingly, the K_a value of **1**⊃**2** is determined to be 9.32×10^3 (± 28%) in CD_3CN.

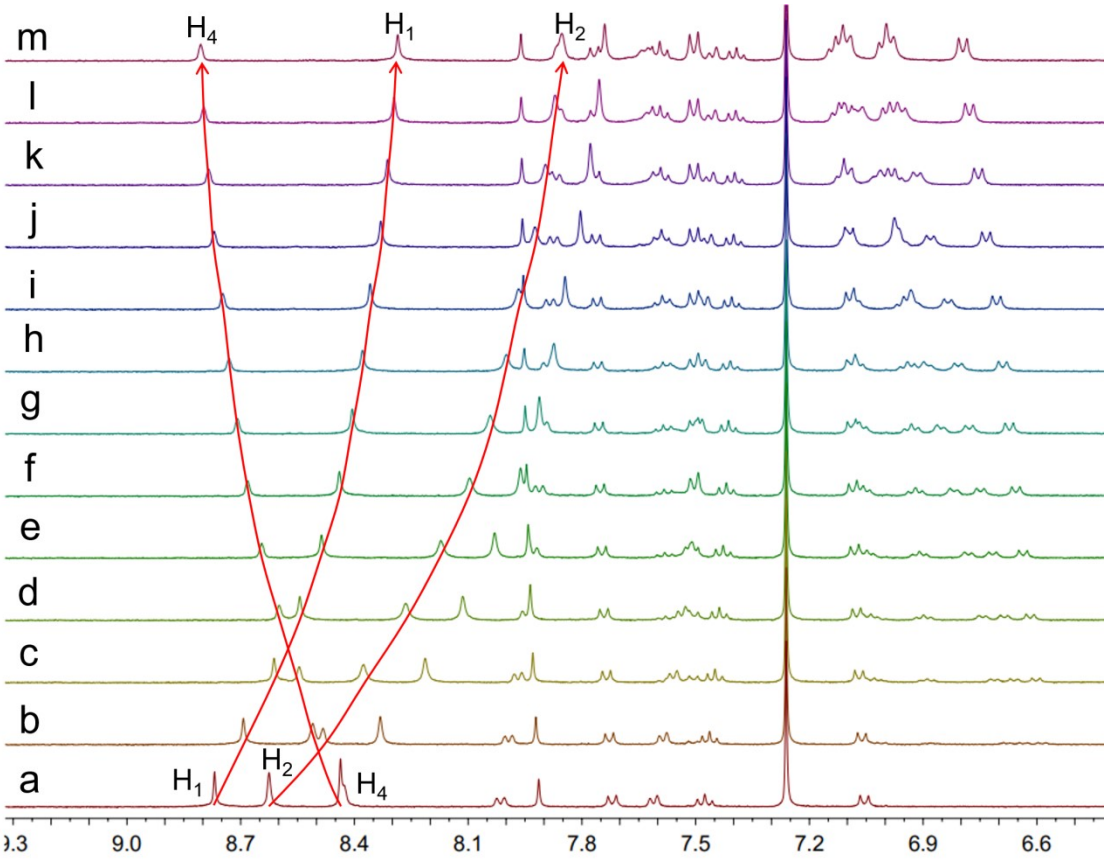

Figure S32. ^1H NMR spectra (400 MHz, $CDCl_3$, 298K) of complex **1**⊃**2** with different molar ratio: a) 0 eq.; b) 0.19 eq.; c) 0.37 eq.; d) 0.54 eq.; e) 0.69 eq.; f) 0.83 eq.; g) 0.97 eq.; h) 1.1 eq.; i) 1.21 eq.; j) 1.43 eq.; k) 1.62 eq.; l) 1.88 eq.; m) 2.10 eq. Obvious chemical shift changes of H_1, H_2 and H_4 are observed for **1** upon addition of **2**, which is able to get the K_d value (see Figure S32).

a

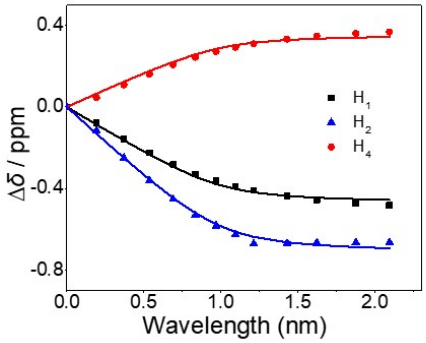

b

1 （mM）	2 (mM)	δ of H1(ppm)	δ of H2(ppm)	δ of H4(ppm)
2.00	0	8.7687	8.6253	8.4367
	0.384615	8.6927	8.5098	8.4832
	0.740741	8.612	8.3751	8.5452
	1.071429	8.5442	8.2646	8.598
	1.37931	8.4869	8.1723	8.6446
	1.666667	8.4396	8.0938	8.6812
	1.935484	8.4057	8.0418	8.7087
	2.1875	8.3788	7.9992	8.7307
	2.424242	8.3584	7.9542	8.7468
	2.857143	8.3304	7.9568	8.7704
	3.243243	8.3125	7.9587	8.7845
	3.75	8.2956	7.9603	8.7973
	4.186047	8.2855	7.961	8.8053

Figure S33. a) Changes of chemical shifts (δ) of protons H_1, H_2, and H_3 on **1** upon addition of **2** (10.00 mM in $CDCl_3$) into **1** (2 mM in $CDCl_3$) at 298 K; b) Data values from the ^{1}H NMR titration experiments (see Figure S32b) of **1**⊃**2** in $CDCl_3$ at 298 K. The solid lines are obtained *via* the Matlab–based global analysis program (fitting program). The K_d value of **1**⊃**2** is determined to be 1.21×10^4 M^{-1} (± 53%) in $CDCl_3$. Accordingly, the K_a value of **1**⊃**2** is determined to be 2.54×10^3 M^{-1} (± 24%).

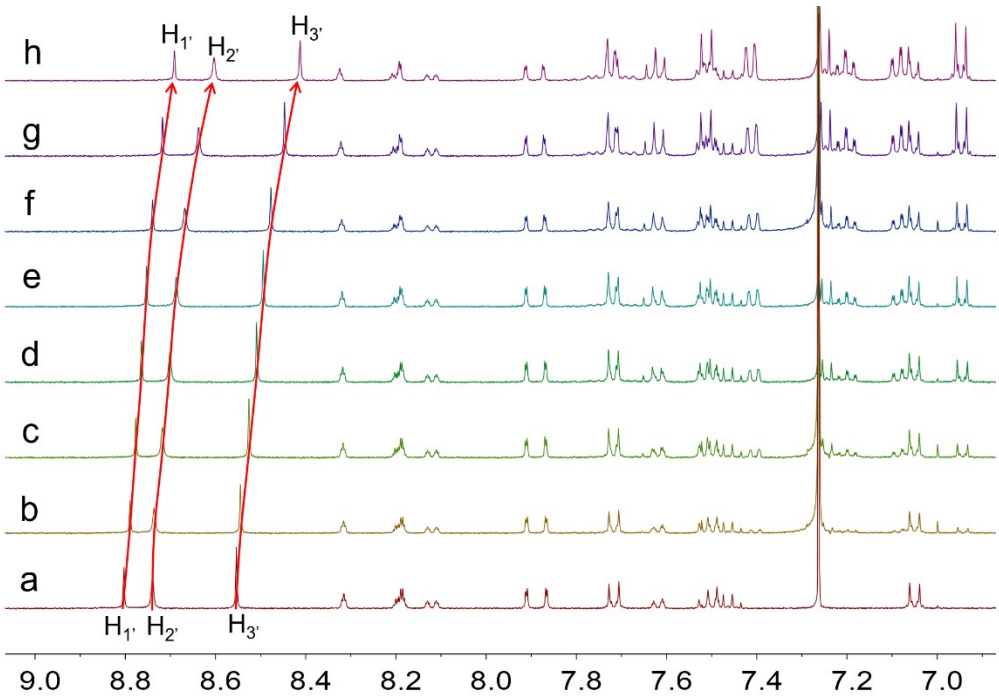

Figure 34. ^{1}H NMR spectra (400 MHz, $CDCl_3$, 298K) of complex **3**⊃**2** with different molar ratio of **2**: a) 0 eq.; b) 0.24 eq.; c) 0.48 eq.; d) 0.72 eq.; e) 0.96 eq.; f) 1.2 eq.; g) 1.68 eq.; h) 2.4 eq. Obvious chemical shift changes of $H_{1'}$, $H_{2'}$ and $H_{3'}$ are observed for **3** upon addition of **2**, which is able to get the K_a value (Figure S34).

a

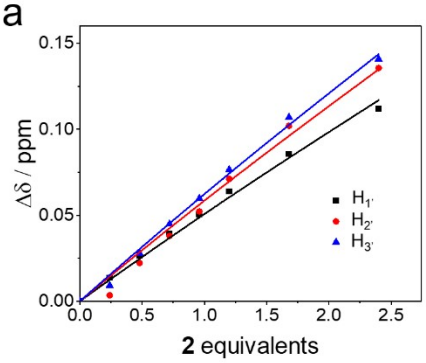

b

3 (mM)	2 (mM)	δ of H1'(ppm)	δ of H2'(ppm)	δ of H3'(ppm)
2.00	0	0	0	0
	0.48	0.0135	0.0034	0.0091
	0.96	0.0262	0.0222	0.028
	1.44	0.0392	0.0379	0.0449
	1.92	0.0504	0.0522	0.0598
	2.4	0.0638	0.0712	0.0766
	3.36	0.0857	0.1021	0.107
	4.8	0.1119	0.1357	0.1409

Figure S35. a) Changes of chemical shifts (δ) of protons $H_{1'}$, $H_{2'}$ and $H_{3'}$ on **3** upon addition of **2** into **3** (2 mM in $CDCl_3$) at 298 K; b) Data values from the ^1H NMR titration experiments (see Figure S35b) of **3**⊃**2** in $CDCl_3$ at 298 K. The solid lines are obtained *via* a Matlab-based global analysis program (fitting program). Accordingly, the K_a value of **3**⊃**2** is determined to be 15.9 M^{-1} (± 167.3%) in $CDCl_3$.

a

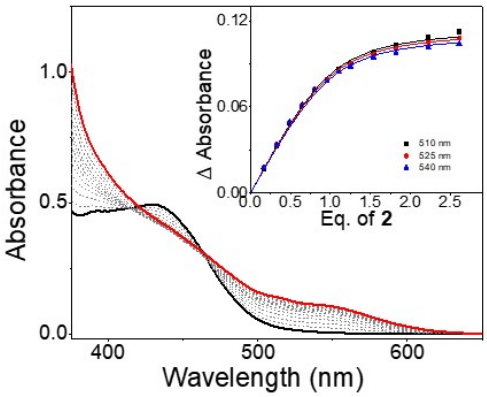

b

1 (mM)	2 (mM)	Abs. (510nm)	Abs. (525nm)	Abs. (540nm)
0.05	0	0.0307769	0.014048	0.0068892
	0.00826446	0.0475299	0.0320724	0.0250712
	0.0163934	0.0635472	0.0479981	0.0408557
	0.0243902	0.0791181	0.0634408	0.0561983
	0.0322581	0.091746	0.0756921	0.0682614
	0.04	0.102939	0.0866593	0.0788996
	0.047619	0.109917	0.0930336	0.08508
	0.0551181	0.116723	0.0995674	0.0911871
	0.0625	0.121368	0.103609	0.0950645
	0.0769231	0.12874	0.110257	0.10108
	0.0909091	0.13367	0.114368	0.104653
	0.111111	0.139195	0.119013	0.108574
	0.130435	0.143271	0.122063	0.110925

Figure S36. a) Changes of UV−Vis absorbance at 510 nm, 525 nm, and 540 nm upon addition of **2** (1.00 mM in CH_3CN) into **1** (0.05 mM in CH_3CN) at 313 K; b) Data values from the UV–Vis titration experiments (see Figure S35b) of **1**⊃**2** in CH_3CN at 313 K. The solid lines are obtained *via* the Matlab–based global analysis program (fitting program). Accordingly, the K_d value of **1**⊃**2** is determined to be 1.73 × 10^5 M^{-1} (± 19%) in CH_3CN at 313 K.

a

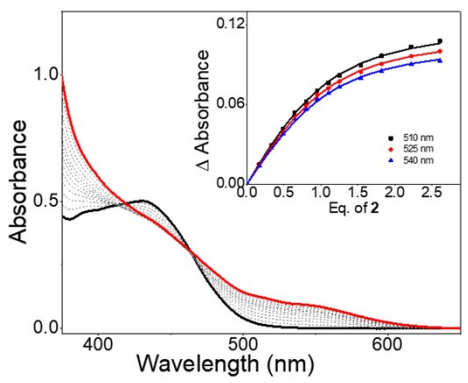

b

1 (mM)	2 (mM)	Abs. (510nm)	Abs. (525nm)	Abs. (540nm)
0.05	0	0.0188587	0.00611151	0.00186814
	0.00826446	0.0335308	0.0204988	0.0155292
	0.0163934	0.0481951	0.0344029	0.0289157
	0.0243902	0.0602934	0.0459859	0.039853
	0.0322581	0.07243	0.0573298	0.0508423
	0.04	0.080995	0.065307	0.0582356
	0.047619	0.0892904	0.0733129	0.0656914
	0.0551181	0.0948704	0.0781701	0.0701831
	0.0625	0.100663	0.0832735	0.0748486
	0.0769231	0.108396	0.0904633	0.0813705
	0.0909091	0.115287	0.0964653	0.0869803
	0.111111	0.122155	0.102376	0.0921118
	0.130435	0.126454	0.106046	0.0947593

Figure S37. a) Changes of UV−Vis absorbance at 510 nm, 525 nm, and 540 nm upon addition of **2** (1.00 mM in CH_3CN) into **1** (0.05 mM in CH_3CN) at 328 K; b) Data values from the UV–Vis titration experiments (see Figure S36b) of **1**⊃**2** in CH_3CN at 328 K. The solid lines are obtained *via* the Matlab–based global analysis program (fitting program). Accordingly, the K_d value of **1**⊃**2** is determined to be 7.11×10^4 M^{-1} (± 8.4%) in CH_3CN at 328 K.

a

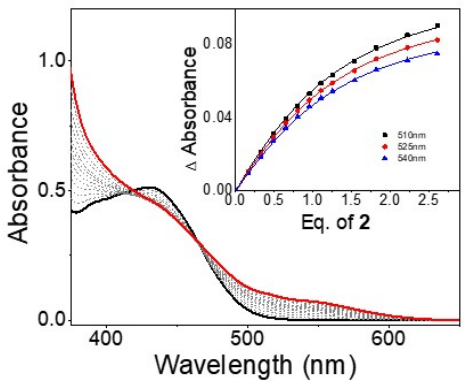

b

1 (mM)	2 (mM)	Abs. (510nm)	Abs. (525nm)	Abs. (540nm)
0.05	0	0.0178401	0.00485164	0.00131983
	0.00826446	0.0284909	0.0155929	0.0113788
	0.0163934	0.0389815	0.0251161	0.0201015
	0.0243902	0.0487694	0.0340905	0.028472
	0.0322581	0.0572112	0.0419922	0.0357071
	0.04	0.0643239	0.0486592	0.0419172
	0.047619	0.0707794	0.0544606	0.0472997
	0.0551181	0.0764009	0.0596021	0.0519733
	0.0625	0.081083	0.0636225	0.0556666
	0.0769231	0.088678	0.070375	0.0616306
	0.0909091	0.0958284	0.0769021	0.0675347
	0.111111	0.102753	0.082896	0.0725242
	0.130435	0.108217	0.087138	0.0760873

Figure S38. a) Changes of UV−Vis absorbance at 510 nm, 525 nm, and 540 nm upon addition of **2** (1.00 mM in CH_3CN) into **1** (0.05 mM in CH_3CN) at 353 K; b) Data values from the UV–Vis titration experiments (see Figure S37b) of **1**⊃**2** in CH_3CN at 353 K. The solid lines are obtained *via* the Matlab–based global analysis program (fitting program). Accordingly, the K_a value of **1**⊃**2** is determined to be 3.21×10^4 M^{-1} (± 5.9%) in CH_3CN.

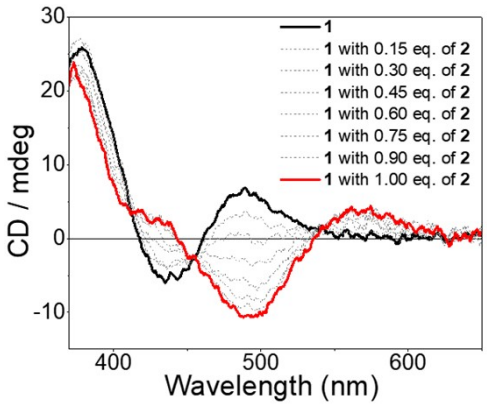

Figure S39. CD spectra changes of **1** upon progressive addition of **2** at 298 K (c = 1.00×10^{-4} M in CH_3CN).

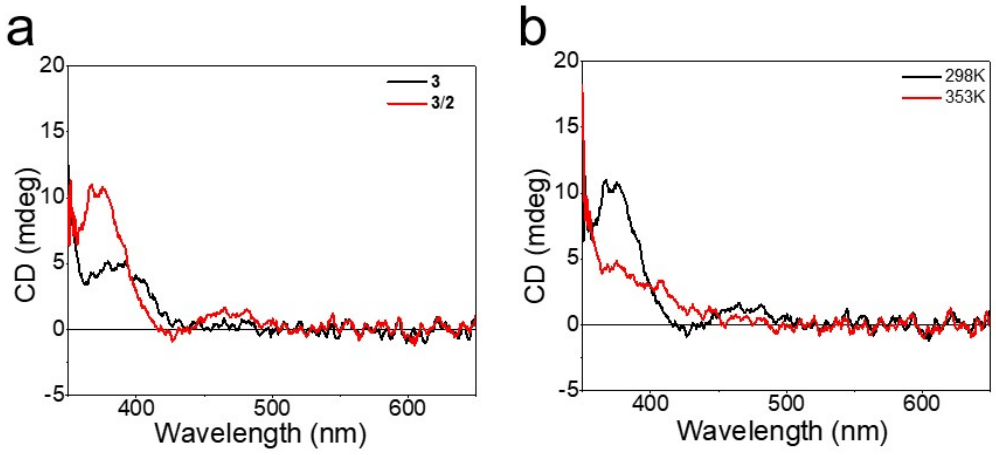

Figure S40. a) CD spectra of **2** and complex **3**⊃**2** (0.10 mM in CH_3CN, 298 K); b) CD spectra of complex **3**⊃**2** (black line) and 353 K (red line) (0.10 mM in CH_3CN). For the complex **3**⊃**2**, supramolecular chirogenic signals at 470 nm disappeared totally at 353 K.

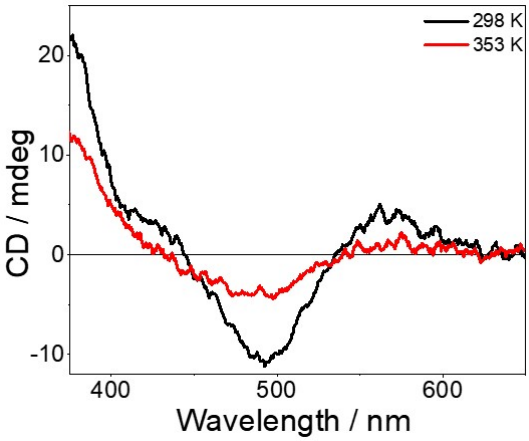

Figure S41. CD spectra of complex **1**⊃**2** (0.10 mM in CH_3CN) at 298 K (black line) and 353 K (red line). The induced CD signals of **1**⊃**2** maintain at elevated temperatures, despite of the decreased CD intensities than that at ambient temperature.

References

[S1] Z. Li, Y. Han, Z. Gao, T. Fu and F. Wang, *Mater. Chem. Front.*, 2018, **2**, 76.
[S2] Y.-K. Tian, Y.-G. Shi, Z.-S. Yang, and F. Wang, *Angew. Chem. Int. Ed.*, 2014, **53**, 6090.
[S3] S. Nueckel and P. Burger, *Organometallics*, 2001, **20**, 4345.
[S4] M. J. Frisch, G. W. Trucks, H. B. Schlegel, G. E. Scuseria, M. A. Robb, J. R. Cheeseman, G. Scalmani, V. Barone, B. Mennucci, G. A. Petersson, H. Nakatsuji, M. Caricato, X. Li, H. P. Hratchian, A. F. Izmaylov, J. Bloino, G. Zheng, J. L. Sonnenberg, M. Hada, M. Ehara, K. Toyota, R. Fukuda, J. Hasegawa, M. Ishida, T. Nakajima, Y. Honda, O. Kitao, H. Nakai, T. Vreven, J. A. Montgomery Jr., J. E. Peralta, F. Ogliaro, M. Bearpark, J. J. Heyd, E. Brothers, K. N. Kudin, V. N. Staroverov, R. Kobayashi, J. Normand, K. Raghavachari, A. Rendell, J. C. Burant, S. S. Iyengar, J. Tomasi, M.

Cossi, N. Rega, J. M. Millam, M. Klene, J. E. Knox, J. B. Cross, V. Bakken, C. Adamo, J. Jaramillo, R. Gomperts, R. E. Stratmann, O. Yazyev, A. J. Austin, R. Cammi, C. Pomelli, J. W. Ochterski, R. L. Martin, K. Morokuma, V. G. Zakrzewski, G. A. Voth, P. Salvador, J. J. Dannenberg, S. Dapprich, A. D. Daniels, O. Farkas, J. B. Foresman, J. V. Ortiz, J. Cioslowski and D. J. Fox, "Gaussian 09," Revision A.1, Gaussian, Inc., Wallingford, 2009.

[S5] L. Szyc, J. Guo, M. Yang, J. Dreyer, P. M. Tolstoy, E. T. J. Nibbering, B. Czarnik-Matusewicz, T. Elsaesser, and H. H. Limbach, *J. Phys. Chem. A*, 2010, **114**, 7749.

[S6] J. S. Chen and R. B. Shirts, *J. Phys. Chem.*, 1985, **89**, 1643.

[S7] a) P. Thordarson, *Chem. Soc. Rev.*, 2011, **40**, 1305; b) A. J. Lowe, F. M. Pfeffer, P. Thordarson, *Supramol. Chem.*, 2012, **24**, 585.

[S8] G. B. W. L. Ligthart, H. Ohkawa, R. P. Sijbesma, and E. W. Meijer, *J. Am. Chem. Soc.*, 2005, **127**, 810.

[S9] (a) S. K. Kim, J. M. Lim, T. Pradhan, H. S. Jung, V. M. Lynch, J. S. Kim, D. Kim, and J. L. Sessler, *J. Am. Chem. Soc.* 2014, **136**, 495*;* (b) M. Yuan, X. Zhang, Y. Han, F. Wang, and F. Wang, *Inorg. Chem.*, 2020*,* **59***,* 14134.

[S10] H. Zhong, S. Jiang, L. Ao, F. Wang, and F. Wang, *Inorg. Chem.*, 2022, **61**, 7111.